東京大学 大学院新領域創成科学研究科
基盤科学研究系
先端エネルギー工学専攻

2021年度
修士論文

Characterization of self-organized structures by the topological constraints

自己組織化における構造決定に係わるトポロジー束縛

2021年7月20日提出
指導委託教員　吉田 善章　教授
指導教員　齋藤　晴彦　准教授

47196118　相原　寛人

Contents

Chapter 1

Introduction

Self-organization in a physical system is a spontaneous process caused by collective dynamics of elements; there is no "blue print" of the structure to be made, but only the rule of interactions among elements dominates the system. For a macroscopic structure to emerge, there is a scale separation between the random motions of the elements and the collective motion of the macro-system, which causes the spontaneous process. In other words, apparently random motion of the elements are restricted by the conservation laws of the macro-system, and the constraint of the macro-system causes the self-organization process.

In this study we focus on two self-organization phenomena: zonal flow in 2D turbulence (part I) and magnetospheric plasma (part II) which are both remarkable phenomena in the context of plasma physics and nuclear fusion. Zonal flow, which is well known in the field of planetary fluid mechanics, also appears in fusion plasma because of the analogy between the geostrophic turbulence and the electrostatic turbulence of magnetized plasma. The reason why zonal flow attracts the attention in the context of plasma physics and nuclear fusion is that it enables us to obtain the quasi-stationary state where thermal gradient is higher. Actually, zonal flow is predicted to be related to H-mode [1] which is well known as a high performance confinement mode in Tokamak [2] although it is still being discussed. On the other hand, magnetospheric plasma is a remarkable example of high-beta plasma confinement which is realized in nature. Here, beta is the ratio of plasma pressure to magnetic pressure which indicates the efficiency of plasma confinement and to realize the

confinement of high-beta plasma is a big issue in nuclear fusion.

The central issue common to these two self-organization phenomena is how the self-organized states are determined. Actually, the basic equations to describe the self-organization phenomena (vorticity equation (3.6) in Chapter 3 and Grad-Shafranov equation (9.4) in Chapter 9, respectively) have infinitely diverse solutions. Then, in reality, how the structure is determined in the process of the self-organization?

Our insight to deal with this problem is that "the constants of motion which constraint the possibility of motion" are the key. For example, in part I, we estimate exact lower bounds on the 'zonal enstrophy', which we consider to be the physical quantity characterizing the trend of self-organization. Here, if we do not take into account any constraints, zonal enstrophy only has trivial lower bound (i.e., zero). However, when we consider appropriate constraint, we obtain nontrivial lower bound. Moreover, the variational principle we formulated to estimate the lower bounds has an unusual mathematical structure which yields nontrivial relation between the lower bound and the constrains. Similarly, to understand the equilibrium state of magnetospheric plasma in part II, considering the appropriate constraints is essential. Under the all degrees of freedom, entropy maximization eliminates any inhomogeneity. Only when we consider some constraints, we obtain nontrivial structure which is consistent with maximum entropy principle.

This paper consists of two parts. In part I, we discuss how strong zonal flow can be in the view of variational principle. This part is based on our paper "Lower bounds on zonal enstrophy" [3]. In part II, which is based on our paper "Kinetic construction of the high-beta anisotropic-pressure equilibrium" [4], we constructed the model to describe magnetospheric high-beta plasma.

Part I

Lower bounds on zonal enstrophy: Self-organization of zonal flow in the view of variational principle

Chapter 2

Introduction of part I

2.1 Background and purpose of part I

The creation of *zonal flow* in the planetary atmosphere is a spectacular example of the self-organization in physical systems [5, 6]. There is a strong analogy between the geostrophic turbulence and the electrostatic turbulence of magnetized plasma in the plane perpendicular to an ambient magnetic field. Because the generation of zonal flow (coherent structure) affects the turbulent transport in magnetized plasmas, how strong it can be is of great interest in the context of plasma confinement [7]. The aim of this work is to estimate exact lower bounds on the "zonal enstrophy" which hence must be satisfied regardless of the dynamics, and elucidate how the lower bounds are determined; lower bounds on the zonal enstrophy indicates that the zonal flow must be stronger than the given value.

The inverse-cascade model explains the essence of the self-organization process. Because of the approximate two-dimensional geometry (due to the scale separation between the shallow vertical direction and wide horizontal directions), the vortex dynamics is free from the stretching effect. Then, the energy of flow velocity tends to accumulate into large-scale vortices, while the enstrophy (the norm of vorticity) cascades to small scales [8]. On a rotating sphere, the gradient of Coriolis force yields the Rossby-wave term in the vortex dynamics equation, which brings about latitude / longitude anisotropy, and the large-scale vorticity form zonal flow [5]. The nonlinear term driving the inverse cascade becomes comparable to the linear Rossby-wave term at the *Rhines scale* which gives a crude estimate

of the latitude size of the zonal flow [9].

While the inverse-cascade model illustrates the general tendency of nonlinear process, the underlying mechanism requires more detailed analysis. The modulational instability plays an essential role in exciting the energy transfer in the wave-number space [10, 11, 12]. In addition to the energy and enstrophy, another quadratic integral is known to be an adiabatic invariant (only changes by fourth-order of perturbations) in the zonal-flow domain of wave-number space, restricting the energy transfer there [13, 14, 15]. Various numerical simulations have been done to demonstrate the creation of zonal flow. Two different categories of models must be distinguished; one is the unforced, free decaying turbulence, and the other is the forced, quasi-stationary turbulence. In the latter case, the interaction between the mean flow and the turbulence [16, 17, 18] or inhomogeneous vorticity mixing [19, 20] have been found as causal mechanisms of zonal flow generation. For these forced, quasi-stationary cases, one has to include some dissipation mechanism for large scale flows in order to remove the energy accumulating in the large scale regime by the inverse cascade. The usual viscosity only works for short scale flows, so something like "friction" is added to the model (however, which mechanism works in a realistic planetary system is still controversial). For the free decaying case, early simulation results [21, 22, 23] demonstrated the self-organization of zonal flow, and found that the scale of zonal flow has similar scaling with Rhines' estimate. However, the quantitative comparison between the Rhines scale and the zonal flow scale was left unclear. On the other hand, in the forced turbulence case, more complex relation has been found, because of the influence of the dissipation mechanism for large scale flows; see [24, 25, 26].

In parallel with simulation studies, there have been theoretical attempts to nail down the "target" of the spontaneous process, i.e. formulating a variational principle that reveals what the dynamics tends to reach. This can be done by identifying the target functional to be minimized (or maximized) as well as the constraints that restrict admissible candidates. A well-known example is the entropy maximization in the microcanonical ensemble (the constraints are total particle number and total energy), which gives the Gibbs distribution. In the application to field theories, where we have to deal with infinite-dimension phase spaces, we encounter the problem of ultraviolet catastrophe (which must be removed by appropriate quantization [27]). Suspending such subtle problems, formal calculations

have been made to obtain the thermal equilibrium distribution of flow fields. In the context of the planetary atmosphere, the statistical equilibrium state in the two-dimensional incompressible Euler system was studied in [28, 29]. In [30], the maximum entropy distribution over the ensemble constrained by total energy and circulation was compared with the large-scale vortex structures observed on Jupiter. However, because of the essential non-equilibrium property of turbulence (as the cascade model is based on "dissipation" in the Kolmogorov microscales, one has to assume a "driving force" to maintain the (quasi) stationary state, or consider a transient process of free decay), the entropy may not be an effective tool to dictate the self-organization.

There is a different type of approach guided by the notion of *selective dissipation* [6]. We begin by making a list of conservation laws that apply in the *ideal* (i.e. dissipation-less) model. A finite dissipation breaks most of the conservation laws. However, there may be differences in fragility among the constants of motion. Here, *fragility* means the sensitivity to small scale perturbations (effective in the Kolmogorov microscale); as the antonym, we say *robust* if the constancy is unaffected by small scale perturbations. We can estimate the fragility by counting the number of spacial derivations included in the ideal constants (see Appendix A). If the most fragile one decreases (or increases) monotonically, we choose it for the target functional, and the others for (approximate) constraints. The minimization (or maximization) may parallel the *relaxation process*; this is, of course, a very crude model of the complex dynamics, assuming that the chosen small-number constants only dictates the relaxation process.

The *Taylor state* of magneto-fluid [31, 32] is the prototype of such a model of self-organization, which minimizes the magnetic field energy ($E = \frac{1}{2}\int |\boldsymbol{B}|^2 \,\mathrm{d}^3x = \frac{1}{2}\int |\nabla \times \boldsymbol{A}|^2 \,\mathrm{d}^3x$, where $\boldsymbol{B} = \nabla \times \boldsymbol{A}$ is the magnetic field) under the constraint on the magnetic helicity ($H = \frac{1}{2}\int \boldsymbol{A}\cdot\boldsymbol{B} \,\mathrm{d}^3x$). The reason why E is more fragile than H is because E includes another differential operator curl in the integrand. This model explains the *relaxed states* of magnetized plasmas in various systems, ranging from laboratory experiments to astronomical objects. Regarding the two dimensional turbulence in the planetary atmosphere, the minimization of the generalized enstrophy (see Proposition 1) under the constraint on the energy has been studied to show that the solution of the minimization problem predicts a steady state with streamlines parallel to contours of the topography [33]. Although these

two stories, i.e. the energy-helicity relation in the magneto-fluid and the enstrophy-energy relation in the 2D-fluid appear to be parallel (as Hasegawa[6] describes in the unified vision), there is a fundamental difference when viewed from their Hamiltonian structures, and the latter needs a careful interpretation. In both systems, the ideal constants (the helicity in magneto-fluids and the enstrophy in 2D-fluids) are Casimirs, by which the orbits are constrained on the level-sets of these constants [34]. In the magneto-fluid phase space, the orbits converge into the equilibrium point as the energy diminishes; the minimum energy (Hamiltonian) state, on each level-set of the helicity, gives an equilibrium point. In the 2D-fluid system, however, the level set of the enstrophy is not embedded as a smooth submanifold in the topology of the energy norm (because the enstrophy is a fragile quantity, its level-set looks like a fractal set; see Appendix A). Hence, we have to reverse the role of the Hamiltonian (energy) and the Casimir (enstrophy), and minimize the enstrophy for a given energy. Then, the critical point is not necessarily an equilibrium point. In this specific problem, however, it is happens to be so, because it is the "maximum point" of the energy. Notice that the minimization of the enstrophy under a constrained energy is equivalent to the maximization of the energy under a constrained enstrophy (see Appendix A). The maximization of the energy appears to be consistent with the inverse-cascade story. However, the simultaneous process, i.e. the forward cascade of the enstrophy violates the constancy of the enstrophy. The dual aspects of the 2D turbulence pose a paradox in the mechanical interpretation of the selective dissipation.

The target of this study is totally different. Whereas we formulate a variational principle using the list of ideal constants of motion, the target functional is not selected from them. We estimate the minimum of the enstrophy possibly given to the zonal component (which we call the *zonal enstrophy*). Knowing how strong the zonal flow must be and how it is controlled is an important issue in the study of turbulent transport. While the total enstrophy is an ideal constant of motion, the zonal part alone is not. We are not proposing that the zonal enstrophy is selectively dissipated; we never provide the target functional with the role of dictating dissipation process Our target functional is simply *what we want to estimate*. We derive an *a priori* estimate of the zonal enstrophy, which must apply to every possible dynamics under a set of prescribed conditions; the ideal invariants are used as such constraints (we do not include the adiabatic invariant, because it

needs the wave number information that is not amenable to our formulation). The actual dynamics is the second subject to be explored, which will be the task of Chapter 5. The analogy of quantum mechanical energy levels may be helpful to explain our perspective. When we want to estimate the energy of an orbital electron, the variational principle to find the critical values of energy, for a fixed total probability, leads us to the eigenvalue problem for the Hamiltonian. The actual energy level that a particular electron will take is determined, for example, by the deexcitation process of emitting photons. We will find a similar picture for the 2D-fluid turbulence; the zonal enstrophy has discrete levels of critical values (local minimums); by emitting wavy enstrophy, the zonal enstrophy relaxes into lower levels.

If there is no constraint on partitioning, the zonal enstrophy can be minimized to zero (even if the total enstrophy is kept at a non-zero constant). But some constraints prevent this to occur. We will identify the "key constraints" that determine the reasonable estimate of the zonal enstrophy.

The reciprocal problem, which maximizes the complementary *wavy enstrophy* (= total enstrophy − zonal enstrophy), was first studied by Shepherd [35] with a different motivation, i.e. to estimate upper bounds on instabilities in nonlinear regime. This is seemingly equivalent to the minimization of the zonal component, however, the effective "constraints" may differ (see Appendix A). The conservation of the *pseudo-momentum* was invoked as the essential constraint. Improved estimates have been proposed by taking into account more general set of invariants which are known as Casimirs [36]. In the present study of the minimization of the zonal component, however, we invoke a different constant of motion, the energy, as the principal constraint (in addition to other ones such as impulse). The physical reason is clear because the self-organization is a spontaneous process in which the redistribution of the enstrophy between the zonal and wavy components can occur only if the energetics admits. Moreover, the energy constraint imparts a mathematically peculiar property to the variational principle, which is the other incentive of this study.

2.2 Outline of part I

Part I is organized as follows. In the next chapter, we will start by reviewing the basic formulation and preliminaries. Chapter 4 describes the main result. We will derive discrete levels of the minimum zonal enstrophy. We will propose the notion of deexcitation to lower enstrophy levels (in analogy of energy levels of quantum states); the relaxation into lower levels corresponds to the inverse cascade. According to the conjecture of Rhines scale [9], the inverse cascade continues until the linear Rossby wave term overcomes the nonlinear term. In Chapter 5, we will study the relaxation process by numerical simulation. The conventional Rhines scale will be revisited to give an improved estimate of the relaxed zonal enstrophy level. Chapter 6 concludes part I.

Chapter 3

Basic formulation and preliminaries

3.1 Vortex dynamics on a beta plane

We consider a barotropic fluid on a beta-plane

$$M = \{\boldsymbol{\xi} = (x, y)^{\mathrm{T}};\, x \in [0, 1), y \in (0, 1)\}.$$

Here, x is the azimuthal coordinate (longitude) and y is the meridional coordinate (latitude). Identifying the points $(0, y)^{\mathrm{T}} = (1, y)^{\mathrm{T}}$, all functions on M is periodic in x. The boundary is $\partial M = \Gamma_0 \cup \Gamma_1$ with

$$\Gamma_0 = \{\boldsymbol{\xi} = (x, 0)^{\mathrm{T}};\, x \in [0, 1)\}, \quad \Gamma_1 = \{\boldsymbol{\xi} = (x, 1)^{\mathrm{T}};\, x \in [0, 1)\}.$$

We will denote the standard L^2 inner product by $\langle f, g\rangle$:

$$\langle f, g\rangle = \int_M f(\boldsymbol{\xi}) g(\boldsymbol{\xi})\, \mathrm{d}^2\xi,$$

and the L^2 norm by $\|f\| = \langle f, f\rangle^{1/2}$.

The state vector is the fluid vorticity $\omega \in L^2(M)$. We define the stream function (or

Gauss potential) ψ by

$$-\Delta\psi = \omega, \tag{3.1}$$

where $\Delta = \partial_x^2 + \partial_y^2$. The flow velocity is given by

$$\boldsymbol{v} = \begin{pmatrix} v_x \\ v_y \end{pmatrix} = \nabla_\perp \psi = \begin{pmatrix} \partial_y \psi \\ -\partial_x \psi \end{pmatrix}. \tag{3.2}$$

Adding a normal coordinate z, we embed x-y plain in $\mathbb{R}^3$, and consider a 3-vector $\tilde{\boldsymbol{v}} = (v_x, v_y, 0)^{\mathrm{T}}$ such that $\partial_z \tilde{\boldsymbol{v}} = 0$. Then, we may calculate $\nabla \times \tilde{\boldsymbol{v}} = (0, 0, -\Delta\psi)^{\mathrm{T}} = (0, 0, \omega)^{\mathrm{T}}$, justifying that we call ω the *vorticity*.

To determine ψ by (3.1), we impose a homogeneous Dirichlet boundary condition

$$\psi\big|_{\Gamma_0} = \psi\big|_{\Gamma_1} = 0. \tag{3.3}$$

Since M is periodic in x, we have

$$D\psi\big|_{x=0} = D\psi\big|_{x=1}, \tag{3.4}$$

where D is an arbitrary linear operator. We note that (3.3) implies that the flow is confined in the domain (i.e. $\boldsymbol{n} \cdot \boldsymbol{v}\big|_{\partial M} = v_y\big|_{\partial M} = 0$; $\boldsymbol{n}$ is the unit normal vector on ∂M), and has zero meridian flux:

$$\int_0^1 v_x \,\mathrm{d}y = \int_0^1 \partial_y \psi \,\mathrm{d}y = \Big[\ \psi\ \Big]_{y=0}^{y=1} = 0. \tag{3.5}$$

We note that a weaker boundary condition such that $\psi|_{\Gamma_0} = a$, $\psi|_{\Gamma_1} = b$ (a and b are some real constants) maintains $v_y|_{\Gamma_0} = v_y|_{\Gamma_1} = 0$, but allows a finite meridian flux (cf. Remark 2).

We define the *Laplacian* as a self-adjoint operator in $L^2(M)$ by imposing the boundary condition (3.3) to its domain. Its unique inverse $\mathcal{K} = (-\Delta)^{-1}$ is a compact self-adjoint operator, by which we can solve (3.1) for ψ.

Taking into account the Coriolis force, the governing equation of ω is

$$\partial_t \omega + \{\omega + \beta y, \psi\} = 0, \tag{3.6}$$

where $\{f, g\} = (\partial_x f)(\partial_y g) - (\partial_x g)(\partial_y f)$, and β is a real constant number measuring the meridional variation of the Coriolis force. When $\beta = 0$, (3.6) reduces into the standard vorticity equation. A finite β introduces anisotropy to the system, resulting in creation of *zonal flow*. The Rhines scale [9] speaks of the balance of the two terms $\{\omega, \psi\}$ and $\{\beta y, \psi\}$, by which we obtain the typical scale length of the zonal flow (see Sec. 4.5)

Inverting (3.1) by $\mathcal{K} = (-\Delta)^{-1}$, we may rewrite (3.6) as

$$\partial_t \omega + \{\omega + \beta y, \mathcal{K}\omega\} = 0. \tag{3.7}$$

We call

$$\omega_t := \omega + \beta y \tag{3.8}$$

the *total vorticity*, which is the sum of the fluid part ω and the ambient part βy (the latter is due to the rotation of the system).

The following identity will be useful in the later calculations:

$$\langle f, \{g, h\} \rangle = \langle g, \{h, f\} \rangle, \tag{3.9}$$

where f, g and h are C^1-class functions in M, and either f or g satisfy (3.3).

Remark 1 (Euler's equation with Coriolis force) The vortex equation (3.6) is derived from Euler's equation of incompressible ($\nabla \cdot \boldsymbol{v} = 0$) inviscid flow with a Coriolis force:

$$\partial_t \boldsymbol{v} + (\boldsymbol{v} \cdot \nabla)\boldsymbol{v} = -\nabla p + 2\boldsymbol{v} \times \boldsymbol{\Omega}, \tag{3.10}$$

where $\boldsymbol{\Omega}$ is the angular velocity of rotating frame, and p is the pressure of the fluid. Putting $2\boldsymbol{\Omega} = \beta y \boldsymbol{e}_z$ ($\boldsymbol{e}_z$ is the unit vector normal to the x-y plane, which we will call the z-direction), assuming a two-dimensional flow (3.2), and operating curl on the both sides of (3.10), we obtain (3.6) from the z-component of the equation. Notice that the Coriolis force is directed perpendicular to $\boldsymbol{v}$, so it does not change the energy of the flow; hence, Coriolis force resembles the Lorentz force $\boldsymbol{v} \times \boldsymbol{B}$.

3.2 Conservation laws and symmetries

Proposition 1 (constants of motion) *The following functionals are constants of motion of the evolution equation (3.7):*

1. *Energy:*

$$E(\omega) := \frac{1}{2}\langle \omega, \mathcal{K}\omega \rangle. \tag{3.11}$$

By rewriting

$$E = \frac{1}{2}\langle (-\Delta\psi), \psi \rangle = \frac{1}{2}\int_M |\nabla\psi|^2 \mathrm{d}^2\xi = \frac{1}{2}\int_M |\nabla_\perp \psi|^2 \mathrm{d}^2\xi = \frac{1}{2}\int_M |\boldsymbol{v}|^2 \mathrm{d}^2\xi,$$

we find that E evaluates the kinetic energy of the flow $\boldsymbol{v}$.

2. *Longitudinal momentum:*

$$P(\omega) := \int_M \partial_y(\mathcal{K}\omega)\, \mathrm{d}^2\xi, \tag{3.12}$$

We may rewrite

$$P = \int_M \partial_y \psi \, \mathrm{d}^2\xi = \int_M v_x \, \mathrm{d}^2\xi$$

to see that P is the integral of the longitudinal momentum. By (3.5), P must be constantly zero.

3. *Circulation:*

$$F(\omega) := \langle 1, \omega \rangle. \tag{3.13}$$

Integrating by parts, we may write

$$F = \int_0^1 \Big[v_x \Big]_{y=0}^{y=1} \mathrm{d}x,$$

which evaluates the circulation of the flow $\boldsymbol{v}$ along the boundary ∂M.

4. *Impulse:*

$$L(\omega) := \langle y, \omega \rangle. \tag{3.14}$$

Integrating by parts and using the boundary conditions (3.3) and (3.4), we may

rewrite

$$L = \int_M y(\partial_x v_y - \partial_y v_x)\,\mathrm{d}^2\xi = \int_M v_x\,\mathrm{d}^2\xi - \int_0^1 \Big[\, y v_x \,\Big]_{y=0}^{y=1} \mathrm{d}x.$$

The first term on the right-hand side is P, which vanishes by (3.5). Hence, L corresponds to the impulse $\boldsymbol{\xi} \times \boldsymbol{v}$ averaged over the boundary.

5. *Generalized enstrophy:*

$$G_\beta(\omega) := \int_M f(\omega + \beta y)\,\mathrm{d}^2\xi, \tag{3.15}$$

where f is an arbitrary C^1-class function, and the argument $\omega + \beta y$ is the total vorticity *including the ambient term βy; see Remark 1. For $f(u) = u^2/2$, $G_\beta(\omega)$ is the conventional enstrophy of the total vorticity.*

6. *Fluid enstrophy:*

$$Q(\omega) := \frac{1}{2}\|\omega\|^2. \tag{3.16}$$

(proof) While these conservation laws are well known, we give the proof to see how they originate. Suppose that ω is a C^1-class solution of (3.7). Rewriting (3.7) in terms of the total vorticity $\omega_t = \omega + \beta y$, we have $\partial_t \omega_t + \{\omega_t, \psi\} = 0$ (where $\psi = \mathcal{K}(\omega_t - \beta y)$).

(1) Using the self-adjointness of $\mathcal{K}$, we may calculate

$$\frac{\mathrm{d}}{\mathrm{d}t}E = \langle \mathcal{K}\omega, \partial_t \omega \rangle = \langle \psi, \{\psi, \omega_t\} \rangle = \langle \omega_t, \{\psi, \psi\} \rangle = 0.$$

(2) To evaluate $\frac{\mathrm{d}}{\mathrm{d}t}P = \int_M (\partial_t v_x)\,\mathrm{d}^2\xi$, we invoke the x-component of Euler's equation $\partial_t \boldsymbol{v} + (\boldsymbol{v}\cdot\nabla)\boldsymbol{v} = -\nabla p + 2\boldsymbol{v} \times \boldsymbol{\Omega}$:

$$\partial_t v_x = -v_x \partial_x v_x - v_y \partial_y v_x + \beta y v_y - \partial_x p.$$

Integrating by parts with the boundary conditions (3.3) and (3.4), we observe

$$\begin{aligned}
\frac{\mathrm{d}}{\mathrm{d}t}P &= \int_M (-v_x \partial_x v_x - v_y \partial_y v_x + \beta y v_y - \partial_x p)\,\mathrm{d}^2\xi \\
&= \int_M \left[-\partial_x (v_x^2 + p) + \beta y v_y\right]\,\mathrm{d}^2\xi \\
&= -\beta \int_0^1 \Big[y\psi \Big]_{x=0}^{x=1} \mathrm{d}y = 0.
\end{aligned}$$

To derive the second line, we have used $\nabla \cdot \boldsymbol{v} = 0$ to put $\partial_y v_y = -\partial_x v_x$.

(3) Using (3.9), we obtain

$$\frac{\mathrm{d}}{\mathrm{d}t}\langle 1, \omega \rangle = \langle 1, \{\psi, \omega_t\} \rangle = \langle \psi, \{\omega_t, 1\} \rangle = 0.$$

(4) Similarly we obtain

$$\begin{aligned} \frac{\mathrm{d}}{\mathrm{d}t} L &= \langle y, \{\psi, \omega + \beta y\} \rangle = \langle y, \{\psi, \omega\} \rangle = \langle \psi, \{\omega, y\} \rangle \\ &= \int_M \psi \, \partial_x \omega \, \mathrm{d}^2\xi = \int_M v_y \omega \, \mathrm{d}^2\xi \\ &= \frac{1}{2} \int_M \partial_x (v_y^2 - v_x^2) \, \mathrm{d}^2\xi = 0. \end{aligned}$$

(5) Using (3.9), we obtain

$$\frac{\mathrm{d}}{\mathrm{d}t} G_\beta = \langle f'(\omega_t), \partial_t \omega_t \rangle = \langle f'(\omega_t), \{\psi, \omega_t\} \rangle = \langle \psi, \{\omega_t, f'(\omega_t)\} \rangle = 0.$$

(6) The generalized enstrophy for $f(u) = u^2/2$ may be written as

$$\begin{aligned} G_\beta(\omega) = \frac{1}{2} \|\omega + \beta y\|^2 &= \frac{1}{2} \|\omega\|^2 + \beta \langle y, \omega \rangle + \frac{\beta^2}{6} \\ &= Q(\omega) + \beta L(\omega) + \frac{\beta^2}{6} \end{aligned}$$

Since $G_\beta(\omega)$ and $L(\omega)$ are constants, $Q(\omega)$ is also a constant.

∎

Remark 2 (Galilean symmetry) Notice that $P \equiv 0$ is an immediate consequence of (3.5) that comes form the homogeneous Dirichlet boundary condition (3.3). However, in the proof of the constancy of P (Proposition 1), we used only $v_y|_{\Gamma_0} = v_y|_{\Gamma_1} = 0$, which may be guaranteed by a weaker boundary condition $\psi|_{\Gamma_0} = a,\ \psi|_{\Gamma_1} = b$ (a and b are some real constants). Hence, in a more general setting of boundary condition (or the definition of $\mathcal{K}$), P may assume a general (non-zero) constant value. Then, a question arises: Dose the homogeneous Dirichlet condition (3.3) violates the generality of vortex dynamics? The answer is no: The Galilean symmetry of the system subsumes the freedom of the foregoing

a and b. First, the transformation $\psi \mapsto \psi - a$ does not change $\boldsymbol{v} = \nabla_\perp \psi$, so we may set a generalized boundary condition to be $\psi|_{\Gamma_0} = 0,\ \psi|_{\Gamma_1} = c$. With $\psi_c := cy$, we decompose $\psi = \psi_0 + \psi_c$ so that ψ_0 satisfies the homogenized boundary condition (3.3). We have $\nabla_\perp \psi_c = c\nabla x$, a constant velocity in the longitudinal direction, and $\omega = -\Delta\psi = -\Delta\psi_0$. Inserting this into (3.6), we obtain

$$\partial_t \omega + \{\omega + \beta y, \psi_0\} + c\{\omega, y\} = 0,$$

The distraction $c\{\omega, y\} = c\partial_x \omega$ can be cleared by Galilean boost $x \mapsto x - ct$. In the inertial frame, we may put $\psi_0 = \mathcal{K}\omega$ to reproduce (3.7).

Evidently, we have

Lemma 1 (translational symmetry) *The constants of motion E, P, F, L, G_β, and W are invariant against the transformation*

$$T(\tau) : \omega(x, y) \mapsto \omega(x + \tau, y), \quad (\tau \in \mathbb{R}). \tag{3.17}$$

3.3 Zonal and wavy components

The phase space of the vorticity ω is

$$V = L^2(M). \tag{3.18}$$

We say that ω is *zonal* when $\partial_x \omega \equiv 0$ in M. The totality of zonal flows deifies a closed subspace $V_z \subset V$. The *zonal average*

$$\mathcal{P}_z \omega := \int_0^1 \omega(x, y)\, \mathrm{d}x \tag{3.19}$$

may be regarded as a projection from V onto V_z. The following basic properties of the projector $\mathcal{P}_z$ may be known to the reader, but we summarize them as Lemmas for the convenience of the analysis in Chapter 4. By the orthogonal decomposition $V = V_z \oplus V_w$,

we define the orthogonal complement V_w, i.e., $\omega_w \in V_w$, iff $\langle \omega_w, \omega_z \rangle = 0$ for all $\omega_z \in V_z$. We call $\omega_w \in V_w$ a *wavy* component, which has zero zonal average: $\mathcal{P}_z \omega_w = 0$. We will denote

$$\mathcal{P}_w = I - \mathcal{P}_z,$$

which is the projector onto V_w. Now we may write

$$V = V_z \oplus V_w = (\mathcal{P}_z V) \oplus (\mathcal{P}_w V).$$

Being projectors, $\mathcal{P}_z$ and $\mathcal{P}_w$ satisfy $\mathcal{P}_z \mathcal{P}_z = \mathcal{P}_z$, $\mathcal{P}_w \mathcal{P}_w = \mathcal{P}_w$, and $\mathcal{P}_z \mathcal{P}_w = \mathcal{P}_w \mathcal{P}_z = 0$. We also have the following useful identity:

Lemma 2 (commutativity) *Let M be a beta-plane (which is periodic in x). For $\psi \in \mathcal{K}(V)$, we have*

$$\mathcal{P}_z \Delta \psi = \Delta \mathcal{P}_z \psi. \tag{3.20}$$

For $\omega \in V$, we have

$$\mathcal{P}_z \mathcal{K} \omega = \mathcal{K} \mathcal{P}_z \omega, \tag{3.21}$$

$$\mathcal{P}_w \mathcal{K} \omega = \mathcal{K} \mathcal{P}_w \omega. \tag{3.22}$$

(proof) By the periodicity in x, we may calculate as

$$\mathcal{P}_z \Delta \psi = \int_0^1 (\partial_x^2 \psi + \partial_y^2 \psi)\, \mathrm{d}x = \Big[\partial_x \psi\Big]_{x=0}^{x=1} + \partial_y^2 \int_0^1 \psi \, \mathrm{d}x = \Delta \mathcal{P}_z \psi.$$

Putting $\psi = \mathcal{K}\omega$, (3.20) reads $-\mathcal{P}_z \omega = \Delta \mathcal{P}_z \mathcal{K} \omega$. Operating $\mathcal{K}$ on both sides yields (3.21). Using this, we obtain $\mathcal{P}_w \mathcal{K} \omega = (1 - \mathcal{P}_z)\mathcal{K}\omega = \mathcal{K}(1 - \mathcal{P}_z)\omega = \mathcal{K}\mathcal{P}_w \omega$.

∎

The following properties are useful:

Lemma 3 (partition laws) *Let us decompose $\omega = \omega_z + \omega_w$ ($\omega_z = \mathcal{P}_z \omega \in V_z$, $\omega_w = \mathcal{P}_w \omega \in V_w$).*

1. *The circulation is occupied by the zonal component ω_z, i.e.,*

$$F(\omega) = F(\omega_z). \tag{3.23}$$

2. *The impulse is occupied by the zonal component ω_z, i.e.,*

$$L(\omega) = L(\omega_z). \tag{3.24}$$

3. *The fluid enstrophy is simply separated as*

$$Q(\omega) = Q(\omega_z) + Q(\omega_w). \tag{3.25}$$

4. *The energy is simply separated as*

$$E(\omega) = E(\omega_z) + E(\omega_w). \tag{3.26}$$

(proof) The first three relations are clear. The energy partition (3.26) is due to

$$\langle \omega_z, \mathcal{K}\omega_w \rangle = \langle \omega_w, \mathcal{K}\omega_z \rangle = 0,$$

which follows from (3.21).

∎

Remark 3 (stationary state) *Evidently, $\partial_x(\mathcal{K}\omega_z) = 0$ for $\omega_z \in V_z$. Hence, $\{\omega_z + \beta y, \mathcal{K}\omega_z\} = 0$, implying that every member $\omega_z \in V_z$ is a stationary solution of (3.7).*

Chapter 4

Estimate of zonal enstrophy

4.1 Zonal enstrophy vs. wavy enstrophy

The aim of this work is to find the minimum of the *zonal enstrophy* defined by

$$Z(\omega) := \frac{1}{2}\|\mathcal{P}_z\omega\|^2. \tag{4.1}$$

The complementary *wavy enstrophy* is $W(\omega) = \frac{1}{2}\|\mathcal{P}_w\omega\|^2$. By (3.25), the total enstrophy is

$$Q(\omega) = Q(\mathcal{P}_z\omega) + Q(\mathcal{P}_w\omega) = Z(\omega) + W(\omega).$$

When the total enstrophy $Q(\omega)$ is conserved (see Proposition 1), the minimum of $Z(\omega)$ gives the maximum of $W(\omega)$.

The simplest version of the minimization problem is to find the minimum $Z(\omega)$ under the constraint of $Q(\omega) = C_Q$ $(\neq 0)$. Introducing a Lagrange multiplier ν, we minimize

$$Z(\omega) - \nu Q(\omega). \tag{4.2}$$

Using the self-adjointness of $\mathcal{P}_z$, we obtain the the Euler-Lagrange equation

$$\mathcal{P}_z\omega - \nu\omega = 0. \tag{4.3}$$

Operating $\mathcal{P}_z$ on (4.3) yields

$$(1-\nu)\mathcal{P}_z\omega = 0.$$

On the other hand, operating $\mathcal{P}_w$ yields

$$\nu\mathcal{P}_w\omega = 0.$$

There are two possibilities of solving these simultaneous equations.

1. $\nu = 0$: Then, $\mathcal{P}_z\omega = \omega_z = 0$ and $\mathcal{P}_w\omega = \omega_w$ is an arbitrary function satisfying $Q(\omega_w) = C_Q$; hence, $\min Z(\omega) = 0$. (This simple exercise reveals an unusual aspect of the present variational principle,which is caused by the *non-coerciveness* of the functional $Z(\omega)$ to be minimized. Notice that the minimizer is not unique, because $\mathcal{P}_z$ has nontrivial kernel, i.e. $\mathrm{Ker}(\mathcal{P}_z) = V_w$).

2. $\nu = 1$: Then, $\mathcal{P}_w\omega = \omega_w = 0$ and $\mathcal{P}_z\omega = \omega_z$ is an arbitrary function satisfying $Q(\omega_z) = Z(\omega) = C_Q$; hence, this solution gives the "maximum" of $Z(\omega)$.

As we mentioned above, the minimizer is not unique here. To obtain a nontrivial estimate of the minimum $Z(\omega)$, we have to take into account "constraints" posed on the dynamics of redistributing enstrophy. Guided by Proposition 1, we start with some simple ones.

4.2 Constraints by circulation and impulse

Let us consider the circulation and impulse as constraints.

Theorem 1 *The minimizer of the zonal enstrophy $Z(\omega)$ under the constraints on the circulation $F(\omega) = C_F$, the impulse $L(\omega) = C_L$, as well as the total enstrophy $Q(\omega) = C_Q$ is a vorticity ω such that*

$$\mathcal{P}_z\omega = a + by, \quad (a = 4C_F - 6C_L,\ b = 12C_L - 6C_F), \tag{4.4}$$

which gives

$$Z_0 := \min Z(\omega) = 2C_F^2 - 6C_FC_L + 6C_L^2. \tag{4.5}$$

(proof) Let us minimize

$$Z(\omega) - \nu Q(\omega) - \mu_0 F(\omega) - \mu_1 L(\omega). \tag{4.6}$$

The Euler-Lagrange equation is

$$\mathcal{P}_z\omega - \nu\omega = \mu_0 + \mu_1 y. \tag{4.7}$$

Operating $\mathcal{P}_z$ on both sides of (4.7) yields

$$(1-\nu)\mathcal{P}_z\omega = \mu_0 + \mu_1 y. \tag{4.8}$$

On the other hand, operating $\mathcal{P}_w$ yields

$$\nu\mathcal{P}_w\omega = 0. \tag{4.9}$$

First, assume that $1-\nu \neq 0$. Inserting $\mathcal{P}_z\omega$ of (4.8) into the definition of $F(\omega) = F(\mathcal{P}_z\omega)$ and $L(\omega) = L(\mathcal{P}_z\omega)$ (see Lemma 3 (1) and (2)), we determine μ_0 and μ_1 of to match the constraint $\langle 1, \omega\rangle = C_F$ and $\langle y, \omega\rangle = C_L$; we obtain $a := \mu_0/(1-\nu) = 4C_F - 6C_L$, and $b := \mu_1/(1-\nu) = 12C_L - 6C_F$. Inserting this $\omega_z = a + by$ into $Z(\omega)$, we obtain the minimum (4.5). On the other hand, (4.9) is satisfied by $\nu = 0$ (consistent with the forgoing assumption $1-\nu \neq 0$) and an arbitrary $\omega_w = \mathcal{P}_w\omega$ such that

$$\frac{1}{2}\|\omega_w\|^2 = C_Q - (2C_F^2 - 6C_F C_L + 6C_L^2). \tag{4.10}$$

The right-hand side is non-negative, if the constraints $F(\omega) = C_F$, $L(\omega) = C_L$ and $Q(\omega) = C_Q$ are consistent. It is only when the constants C_F, C_L and C_Q are given so that the right-hand side of (4.10) is zero, that the other assumption $1-\nu = 0$ applies; then, the unique solution $\mathcal{P}_w\omega = 0$ (hence, $\omega = \mathcal{P}_z\omega$) is obtained.

∎

Notice that the minimizer is still non-unique (excepting the special case mentioned in the proof); every $a + by + \omega_w$ ($\forall\omega_w \in V_w$ such that (4.10) holds) satisfies (4.4). However,

the minimum value (4.5) is uniquely determined.

4.3 Constraint by energy

The situation changes dramatically, when we include the energy constraint $E(\omega) = C_E$; laminated vorticity distribution, epitomizing the structure of zonal flow, is created by the energy constraint. The number of lamination (jet number) is identified by the "eigenvalue" of the Euler-Lagrange equation, which specifies the "level" of the zonal enstrophy (in analogy of the quantum number of discrete energy in quantum mechanics). To highlight the role of the energy constraint, we first omit the constraints on the circulation and impulse.

Taking into account the energy and total enstrophy constraint, we seek the critical points of

$$Z(\omega) - \nu Q(\omega) - \mu_2 E(\omega).$$

The Euler-Lagrange equation is

$$\mathcal{P}_z\omega - \nu\omega - \mu_2\mathcal{K}\omega = 0. \tag{4.11}$$

Operating $\mathcal{P}_z$ yields (denoting $\omega_z = \mathcal{P}_z\omega$)

$$\omega_z - \nu\omega_z - \mu_2\mathcal{K}\omega_z = 0. \tag{4.12}$$

On the other hand, $\omega_w = \mathcal{P}_w\omega$ must satisfy

$$\nu\omega_w + \mu_2\mathcal{K}\omega_w = 0. \tag{4.13}$$

Putting $\omega_z = -\partial_y^2\psi_z(y)$ in (4.12), we obtain

$$\partial_y^2\psi_z + \lambda^2\psi_z = 0, \quad \lambda^2 = \frac{\mu_2}{1-\nu}. \tag{4.14}$$

The solution satisfying the boundary conditions $\psi_z(0) = \psi_z(1) = 0$ is

$$\psi_z = A \sin \lambda y \tag{4.15}$$

with eigenvalues

$$\lambda = n_1 \pi \ (n_1 \in \mathbb{Z}).$$

The corresponding zonal vorticity is

$$\omega_z = A\lambda^2 \sin \lambda y. \tag{4.16}$$

On the other hand, putting $\omega_w = -\Delta\psi_w$, (4.13) reads

$$\Delta\psi_w + k^2\psi_w = 0, \quad k^2 = -\frac{\mu_2}{\nu}. \tag{4.17}$$

The solution satisfying the boundary conditions $\psi_w(x, 0) = \psi_w(x, 1) = 0$, as well as the periodicity in x, is given by (as the equivalent class of the translational symmetry in x; see Lemma 1)

$$\psi_w = B \sin k_x x \ \sin k_y y, \quad k^2 = k_x^2 + k_y^2 \tag{4.18}$$

with eigenvalues

$$k_x = 2n_2\pi, \ k_y = n_3\pi \ (n_2, \ n_3 \in \mathbb{Z}).$$

The corresponding wavy vorticity is

$$\omega_w = Bk^2 \sin k_x x \ \sin k_y y. \tag{4.19}$$

Summing the zonal and wavy components, we obtain

$$\psi = A \sin \lambda y + B \sin k_x x \ \sin k_y y, \tag{4.20}$$

$$\omega = A\lambda^2 \sin \lambda y + Bk^2 \sin k_x x \ \sin k_y y. \tag{4.21}$$

The two amplitudes A and B are determined by the constraints $E(\omega) = C_E$ and $Q(\omega) =$

C_Q; inserting (4.20) and (4.21) into the definitions of $E(\omega)$ and $Q(\omega)$, we obtain

$$C_E = \frac{A^2\lambda^2}{4} + \frac{B^2k^2}{8}, \tag{4.22}$$

$$C_Q = \frac{A^2\lambda^4}{4} + \frac{B^2k^4}{8}. \tag{4.23}$$

Solving (4.22) and (4.23) for A and B, and inserting the solution into the zonal enstrophy $Z(\omega)$ and wavy enstrophy $W(\omega)$, we obtain the critical values

$$Z_{\lambda,\epsilon} = \frac{\lambda^2 C_E - \epsilon C_Q}{1-\epsilon}, \tag{4.24}$$

$$W_{\lambda,\epsilon} = \frac{C_Q - \lambda^2 C_E}{1-\epsilon}, \tag{4.25}$$

where $\epsilon = \lambda^2/k^2$, scaling the ratio of the wave length of the zonal components to that of the wavy components. For $Z_{\lambda,\epsilon} \geq 0$ and $W_{\lambda,\epsilon} \geq 0$, there are two possibilities: $\epsilon \leq (\lambda^2 C_E)/C_Q \leq 1$ or $\epsilon \geq (\lambda^2 C_E)/C_Q \geq 1$. Here, the former regime of ϵ is relevant, because we assume that the wavy components have smaller scales in comparison with the zonal component (i.e. $\epsilon < 1$). Then, $Z_{\lambda,\epsilon}$ of (4.24) increases monotonically as ϵ decreases (or k^2 increases; see Fig. 4.1), and we have

$$\lim_{\epsilon \to 0} Z_{\lambda,\epsilon} = \lambda^2 C_E. \tag{4.26}$$

Notice that this limit gives the upper bound for $Z(\omega)$ of the corresponding eigenvalue λ, which is achieved when the wavy component has the smallest scale $\epsilon \to 0$. For actual wavy components, $Z(\omega)$ takes a smaller value than $\lambda^2 C_E$, i.e.

$$Z(\omega) \leq \lambda^2 C_E. \tag{4.27}$$

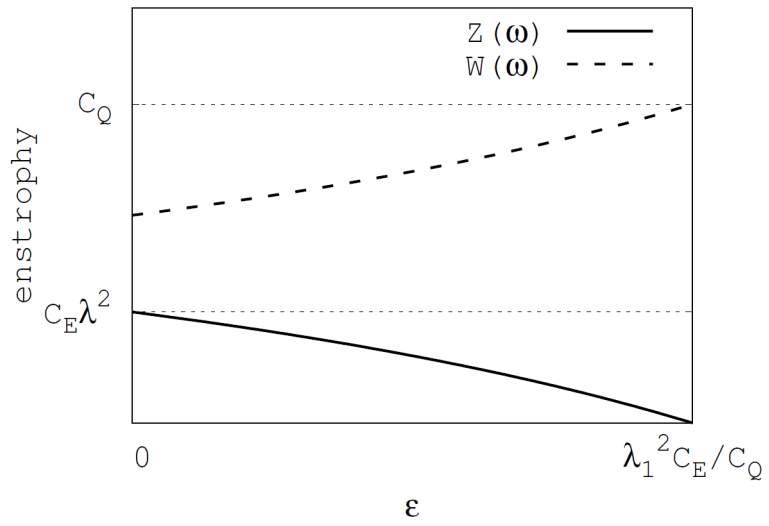

Figure 4.1: The graph of $Z(\omega)$ and $W(\omega)$ given in (4.24) and (4.25).

4.4 Constraints by energy, circulation, impulse and total enstrophy

Now we study the minimum of the zonal enstrophy $Z(\omega)$ under the all constraints of energy, circulation, impulse, and total enstrophy. In contrast to the observation of Sec. 4.3 (where the minimum of $Z(\omega)$ is not determined by the energy C_E), we will find that the minimum of $Z(\omega)$ is determined by the circulation C_F and impulse C_L. In comparison with the result of Sec. 4.2, however, we have a discrete set of enstrophy levels (each of them corresponds to different lamination number of zonal flow). Whereas they are due to the energy constraint, $Z(\omega)$ itself does not depend on the values of the energy C_E.

Introducing Lagrange multipliers, we seek the minimizer of

$$Z(\omega) - \nu Q(\omega) - \mu_0 F(\omega) - \mu_1 L(\omega) - \mu_2 E(\omega).$$

The Euler-Lagrange equation is

$$\mathcal{P}_z \omega - \nu\omega - \mu_0 - \mu_1 y - \mu_2 \mathcal{K}\omega = 0. \tag{4.28}$$

The solution satisfying the boundary conditions $\psi(x,0) = \psi(x,1) = 0$, as well as the periodicity in x, is $\psi = \psi_z + \psi_w$ with

$$\psi_z = A_1 \cos \lambda y + A_2 \sin \lambda y - \frac{\mu_0 + \mu_1 y}{\mu_2}, \tag{4.29}$$

$$\psi_w = B \sin k_x x \ \sin k_y y, \tag{4.30}$$

where

$$\lambda = \sqrt{\frac{\mu_2}{1-\nu}}, \quad k^2 = k_x^2 + k_y^2 = -\frac{\mu_2}{\nu}, \tag{4.31}$$

and

$$k_x = 2n_2\pi, \ k_y = n_3\pi \ (n_2, \ n_3 \in \mathbb{Z}). \tag{4.32}$$

The corresponding vorticities are

$$\omega_z = A_1\lambda^2 \cos \lambda y + A_2\lambda^2 \sin \lambda y. \tag{4.33}$$

$$\omega_w = Bk^2 \sin k_x x \ \sin k_y y. \tag{4.34}$$

The zonal enstrophy $Z(\omega)$ of the minimizer is

$$\begin{aligned} Z(\omega) &= \frac{A_1^2\lambda^3}{8}(2\lambda + \sin 2\lambda) + \frac{A_2^2\lambda^3}{8}(2\lambda - \sin 2\lambda) \\ &\quad + \frac{A_1 A_2 \lambda^3}{4}(1 - \cos 2\lambda). \end{aligned} \tag{4.35}$$

We have yet to determine the eigenvalue λ and the coefficients A_1, A_2 and B. Inserting $\psi = \psi_z + \psi_w$ and $\omega = \omega_z + \omega_w$ into the constraints $F(\omega) = C_F$, $L(\omega) = C_L$, $E(\omega) = C_E$

and $Q(\omega) = C_Q$, we obtain

$$\begin{aligned}
C_F &= A_1\lambda\sin\lambda + A_2\lambda(1-\cos\lambda), && (4.36)\\
C_L &= A_1(\lambda\sin\lambda + \cos\lambda - 1) + A_2(\sin\lambda - \lambda\cos\lambda), && (4.37)\\
C_E &= \frac{A_1^2\lambda}{8}(2\lambda + \sin 2\lambda) + \frac{A_2^2\lambda}{8}(2\lambda - \sin 2\lambda)\\
&\quad + \frac{A_1A_2\lambda}{4}(1-\cos 2\lambda) - \frac{A_1C_F}{2}\\
&\quad - \frac{[A_1(\cos\lambda - 1) + A_2\sin\lambda]C_L}{2} + \frac{B^2k^2}{8}, && (4.38)\\
C_Q &= \frac{A_1^2\lambda^3}{8}(2\lambda + \sin 2\lambda) + \frac{A_2^2\lambda^3}{8}(2\lambda - \sin 2\lambda)\\
&\quad + \frac{A_1A_2\lambda^3}{4}(1-\cos 2\lambda) + \frac{B^2k^4}{8}. && (4.39)
\end{aligned}$$

We may write (4.36) and (4.37) as

$$\begin{pmatrix} C_F \\ C_L \end{pmatrix} = \mathrm{D}(\lambda) \begin{pmatrix} A_1 \\ A_2 \end{pmatrix}. \tag{4.40}$$

with

$$\mathrm{D}(\lambda) := \begin{pmatrix} \lambda\sin\lambda & \lambda(1-\cos\lambda) \\ \lambda\sin\lambda + \cos\lambda - 1 & \sin\lambda - \lambda\cos\lambda \end{pmatrix}. \tag{4.41}$$

For given C_F and C_L, we solve (4.40) to determine the amplitudes of zonal vorticity:

$$\begin{aligned}
A_1 &= \frac{C_F(\sin\lambda - \lambda\cos\lambda) + C_L(-\lambda + \lambda\cos\lambda)}{\det D(\lambda)}, && (4.42)\\
A_2 &= \frac{C_F(-\lambda\sin\lambda - \cos\lambda + 1) + C_L\lambda\sin\lambda}{\det D(\lambda)}, && (4.43)
\end{aligned}$$

where $\det D(\lambda) = \lambda(2 - \lambda\sin\lambda - 2\cos\lambda)$. Inserting (4.42) and (4.43) into (4.35), we obtain the zonal enstrophy evaluated as a function of λ, which we denote by Z_λ. The critical points (local minimums) of $Z(\omega)$, given by

$$\frac{\mathrm{d}}{\mathrm{d}\lambda} Z_\lambda = 0, \tag{4.44}$$

determine the eigenvalues λ characterizing the *enstrophy levels*.

Instead of displaying the lengthy expression of Z_λ, we will show its graphs for typical choices of the parameters C_F and C_L. Notice that Z_λ depends only on C_F (circulation) and C_L (impulse); it does not contain C_E (energy) and C_Q (enstrophy) as parameters. First, we pay attention to the singularities given by $\det D(\lambda) = 0$, where $A_1 \to \infty$ and $A_0 \to \infty$, hence $Z_\lambda \to \infty$ (there is an exception, as discussed later). We show the graph of $\det D(\lambda)$ in Fig. 4.2.

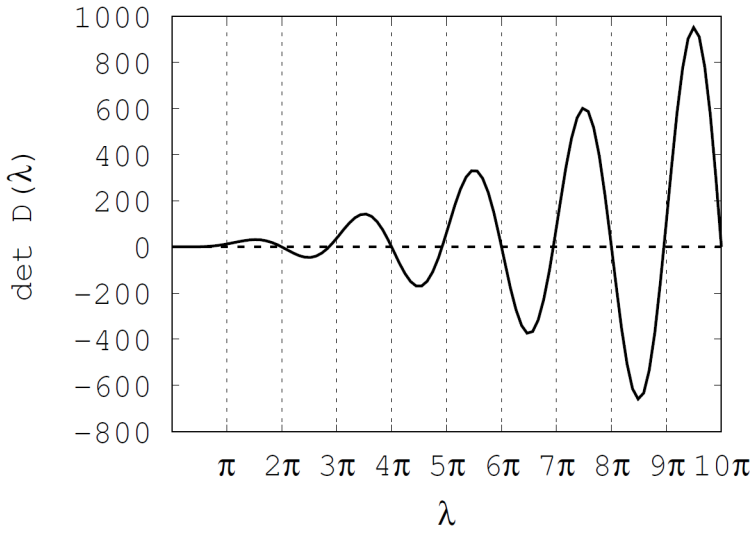

Figure 4.2: The graph of $\det D$.

There are two types of solutions:

$$\lambda = \begin{cases} \Lambda_{2n} = 2n\pi, \\ \Lambda_{2n+1} = (2n+1)\pi - \delta_n, \end{cases} \qquad (n = 0, 1, \cdots),$$

where each δ_n is a small positive number such that $\delta_n \to 0$ as $n \to \infty$. The minimums of Z_λ appear in every interval $(\Lambda_{2n}, \Lambda_{2n+1})$. However, if $C_F = 2C_L$, Z_λ remains finite at $\lambda = \Lambda_{2n+1}$. In this special case, the minimums of Z_λ appear in intervals $(\Lambda_{2n}, \Lambda_{2n+2})$.

In Fig. 4.3, we show examples of Z_λ calculated for (left) $C_F = 0.28$ and $C_L = 0.07$, (right) $C_F = 0.28$ and $C_L = 0.14$ ($C_F = 2C_L$).

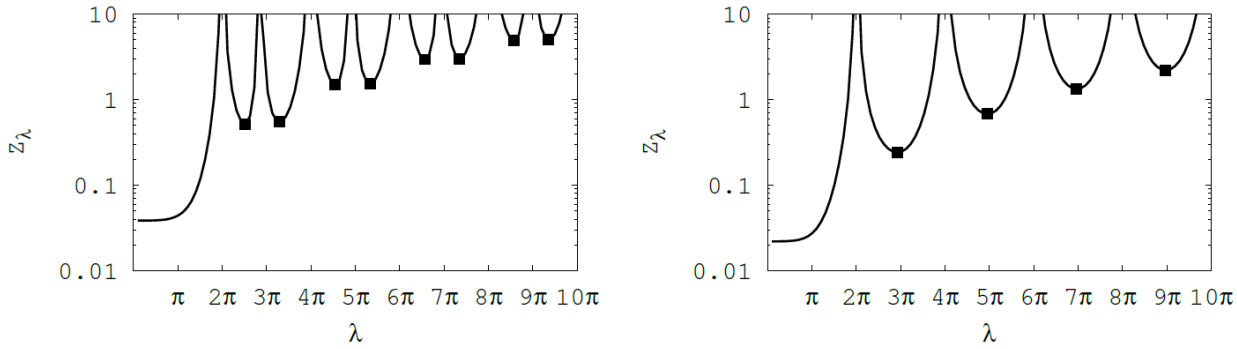

Figure 4.3: The graphs of the critical zonal enstrophy Z_λ as functions of λ. The minimums of Z_λ determine the eigenvalues of λ. The points on the curve indicates the eigenvalues. We assume (left) $C_F = 0.21$ and $C_L = 0.0525$, and (right) $C_F = 0.21$ and $C_L = 0.105$.

At $\lambda = 0$, Z_λ reproduces the result of Theorem 1, i.e.

$$\lim_{\lambda \to 0} Z_\lambda = Z_0 = 2C_F^2 - 6C_F C_L + 6C_L^2, \tag{4.45}$$

which is the absolute minimum of the zonal enstrophy under the constraints on the circulation $F(\omega) = C_F$, the impulse $L(\omega) = C_L$, and the total enstrophy $Q(\omega) = C_Q$.

The role of the energy constraint $E(\omega) = C_E$ is to create eigenvalues of λ at which Z_λ takes *local minimum* values. However, the value of C_E does not influence the value of Z_λ directly. As we have seen in (4.27), it poses a constraint on the maximum:

$$Z(\omega) \leq \lambda^2 C_E, \tag{4.46}$$

in addition to the other implicit constraint $Z(\omega) \leq C_Q$. Instead of the zonal component ω_z of (4.33), C_E and C_Q work for determining the complementary wavy component ω_w of (4.34). By (4.38) and (4.39), we obtain

$$k^2 = \frac{C_Q - Z_\lambda}{C_E - E_{z,\lambda}}, \tag{4.47}$$

$$B^2 = \frac{8(C_E - E_{z,\lambda})^2}{C_Q - Z_\lambda}, \tag{4.48}$$

where $E_{z,\lambda}$ is the energy of the zonal component ω_z evaluated at the eigenvalue λ. Notice that k^2B^2 ($\sim$ energy of the wavy component) is determined only by C_E and $E_{z,\lambda}$. So, the role of the total enstrophy constraint is to determine the wave number k of the wavy component.

Remark 4 (trivial constraints) For the special case of $C_F = 0$ and $C_L = 0$, a laminated zonal flow ($A_1 \neq 0$ and/or $A_2 \neq 0$) can occur only if

$$\det D(\lambda) = \lambda(2 - \lambda \sin\lambda - 2\cos\lambda) = 0.$$

Then, the eigenvalues are $\lambda = \Lambda_{2n}$ and Λ_{2n+1} ($n = 0, 1, 2, \cdots$), the previous singular points; see Fig. 4.2. For $\lambda = \Lambda_{2n}$ ($\lambda = 0$ gives the trivial solution $\omega_z = 0$),

$$\mathrm{D}(\lambda) = \begin{pmatrix} 0 & 0 \\ 0 & -\lambda \end{pmatrix},$$

hence, $A_2 = 0$. On the other hand, for $\lambda = \Lambda_{2n+1}$,

$$\mathrm{D}(\lambda) = \frac{1}{4}\lambda \sin\lambda \begin{pmatrix} 4 & 2\lambda \\ 2 & \lambda \end{pmatrix},$$

and then $A_2 = -2A_1/\Lambda_{2n}$. In both cases, A_1 is arbitrary, so we cannot determine the amplitude of the zonal vorticity ω_z. Therefore, the trivial conditions $C_F = 0$ and $C_L = 0$ reproduce the situation of "no-constraint" discussed in Sec. 4.3. We only have the estimate of the maximum (4.27).

The forgoing results are summarized as:

Theorem 2 *For a given set of constants $F(\omega) = C_F$, $L(\omega) = C_L$, $E(\omega) = C_E$, and $Q(\omega) = C_Q$, the zonal enstrophy $Z(\omega)$ has a discrete set of critical (local minimum) values quantized by the eigenvalue λ measuring the lamination period of the zonal vorticity.*

1. *When $C_F \neq 0$ or $C_L \neq 0$, the eigenvalue λ is given by (4.44) as a function of C_F and C_L. The corresponding eigenfunction ω_z, and the critical value of $Z(\omega)$ are*

determined by C_F and C_L; see (4.33), (4.35), (4.42) and (4.43). The other constants C_E and C_Q determine upper bounds $C_E\lambda^2 \geq Z(\omega)$ and $C_Q \geq Z(\omega)$.

2. *For the special values $C_F = C_L = 0$, additional eigenvalues $\lambda = 2n\pi$ and $\lambda = \Lambda_n$ ($n = 1, 2, \cdots$) occur. However, the eigenfunctions ω_z and the critical values of $Z(\omega)$ are no longer determined by such C_F and C_L; we only have estimates of upper bounds $C_E\lambda^2 \geq Z(\omega)$ and $C_Q \geq Z(\omega)$.*

4.5 Determination of the zonal enstrophy level

To apply Theorem 2 to the estimation of attainable zonal enstrophy, we have to determine the eigenvalue λ that identifies the zonal enstrophy level. Here, we suggest the following method (which we will examine and improve in Chapter 5).

The self-organization of zonal flow can be seen as a relaxation process of the zonal enstrophy level, which parallels the inverse cascade in the meridional wave number space. Just as the transition of the quantum energy level is caused by photon emission, the relaxation of the zonal enstrophy level is due to the emission of wavy vorticity, which is driven by the nonlinear coupling of the zonal and wavy components. Therefore, the relaxation can proceed as far as the nonlinear term $\{\omega, \psi\}$ dominates the evolution equation (3.6). Relative to the concomitant linear term $\beta\{y, \psi\}$, the nonlinear term becomes weaker as the length scale increases (i.e., the inverse cascade proceeds). On the Rhines scale [9]

$$L_R = \sqrt{\frac{2U}{\beta}}, \tag{4.49}$$

the linear and nonlinear terms have comparable magnitudes, where U is the representative magnitude of the zonal flow velocity.

Since the energy is conserved, we may estimate $U = \sqrt{2C_E}$. Hence, we have an *a priori* estimate

$$\lambda \sim \frac{\pi}{L_R} = \pi\sqrt{\frac{\beta}{2\sqrt{2C_E}}}. \tag{4.50}$$

Notice the influence of the energy C_E on the eigenvalue λ. Although each value of the zonal enstrophy level is independent to C_E, the selection of the level is made by C_E.

Chapter 5

Comparison with numerical simulations

5.1 Simulation model

In this chapter, we compare the forgoing theoretical estimates with numerical simulation results. With a system size L and a rotation period T, we normalize the variables as

$$\check{x} = \frac{x}{L},\ \check{y} = \frac{y}{L},\ \check{t} = \frac{t}{T},\ \check{\omega} = \omega T,\ \check{\psi}\ = \frac{\psi T}{L^2}, \tag{5.1}$$

by which the vorticity equation reads

$$\partial_{\check{t}}\check{\omega} + \{\check{\omega} + \beta\check{y}, \check{\psi}\} = \nu\nabla\check{\omega}, \tag{5.2}$$

where ν represents the viscosity (reciprocal Reynolds number). For simplicity, we will omit the normalization symbol $\check{}$ in the following description. Whereas our theoretical analysis is based on the dissipation-free model (3.6), we add a finite viscosity ν for numerical stability (typically, we put $\nu = 1.0 \times 10^{-6}$). A finite viscosity is also indispensable for the self-organization process, because the ideal (zero viscosity) dynamics is constrained by infinite number of Casimirs (local circulations), preventing changes in streamline topology. The theoretical model, however, ignores the dissipation by assuming the robustness of the invariants that are used as constraints (see Proposition 1). The influence of dissipation

will be examined carefully when we compare the theory and numerical simulation.

In the following simulation, we assume parameters comparable to the Jovian atmosphere, where $L = 4.4 \times 10^8$m, $T = 8.6 \times 10^5$sec. The parameter β is determined as

$$\beta = \frac{2\Omega}{R}(\cos\theta)LT,$$

where Ω is the angular vorticity of rotating frame and R is the radius and θ is latitude. For $L \sim 2\pi R$ and $\theta \sim 0$, we obtain $\beta \sim 10^2$. The jet velocity reaches $U \sim 1 \times 10^2$ m/s, which yields $C_F \sim 4 \times 10^{-1}$ and $C_L \sim 2 \times 10^{-1}$ if the jet achieves the maximum opposite velocities on both north and south boundaries. Here we assume moderate values $C_F \sim 10^{-1}$ and $C_L \sim 10^{-1}$.

Remark 5 (General aspect ratio) When we consider a rectangular domain with a general aspect ratio α (the system size in y is L, while in x is αL, and T is a rotation period), variables are normalized as

$$\check{x} = \frac{x}{\alpha L},\ \check{y} = \frac{y}{L},\ \check{t} = \frac{t}{T},\ \check{\omega} = \frac{\omega}{\Omega},\ \check{\psi}\ = \frac{\psi}{\Psi}, \tag{5.3}$$

with

$$\Omega = \frac{1}{T},\ \Psi = \frac{L^2}{T},\ \check{\nu} = \frac{\nu T}{L^2},\ \check{\beta} = \beta LT, \tag{5.4}$$

the governing equation (3.6) modifies as

$$\partial_{\check{t}}\check{\omega} + \frac{1}{\alpha}\{\check{\omega} + \check{\beta}\check{y}, \check{\psi}\} = 0, \tag{5.5}$$

where

$$-(\frac{1}{\alpha^2}\frac{\partial^2}{\partial\check{x}^2} + \frac{\partial^2}{\partial\check{y}^2})\check{\psi} = \check{\omega}. \tag{5.6}$$

While $\alpha \neq 1$ changes the relation between ψ and ω, it does not influence the results of Theorem 1 and Theorem 2, because the zonal component of the solution ω_z (or ψ_z) of the Euler-Lagrange equation is invariant. The Rhines scale is also independent to α. So, we assume $\alpha = 1$.

5.2 Self-organized zonal flow

As we have seen, the theoretical estimate of the minimum $Z(\omega)$ changes dramatically depending on whether C_F and C_L are finite or not (Sec. 4.4). First, we study the general case where both C_F and C_L are finite (the special case of $C_F = 0$ and $C_L = 0$ will be examined in Sec. 5.4). We assume an initial condition such that

$$\omega|_{t=0} = 5.0 \sin 15\pi y + \sum_{m,n} \alpha_{mn} e^{imx} \sin n\pi y,$$

with random $\alpha_{mn}(|\alpha_{mn}| \in [0, 50)$ for $5 \leq m, n \leq 10)$, which yields $C_E = 3.6 \times 10^{-2}$, $C_F = 0.21$ and $C_L = 0.105$.

In Fig. 5.1, we show the evolution of the "ideal" constants. The total energy C_E is well conserved. The changes in C_F and C_L are also tolerable. Because of a finite viscosity ($\nu = 1.0 \times 10^{-6}$), however, the total enstrophy C_Q changes significantly. But it is not essential for the present purpose of comparison, because the theoretical estimate of minimum $Z(\omega)$ is independent of the C_Q. As noted after (4.47)-(4.48), the total enstrophy $Q(\omega) = C_Q$ only contributes to estimating the wave number k of the wavy component ω_w. As the simulation shows, the "dissipation" of the total enstrophy is the signature of the relaxation, when we consider a finite viscosity. We may interpret the dissipation as the scale separation between the visible scale and micro scale; the latter is separated from the vortex dynamics model by suppressing the amplitudes of micro-scale vortices. This scenario is consistent with the local interaction model; the nonlinear dynamics is dominated by interactions among similarly sized vortices (i.e., local in the Fourier space) within the inertial range, so it is not influenced by vortices of far smaller scales.

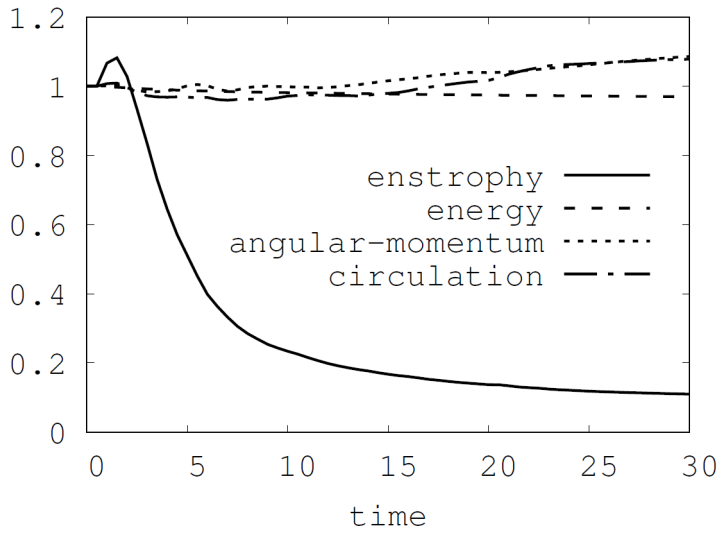

Figure 5.1: The evolution of the "ideal" constants in the simulation. Each value is normalized by the corresponding initial value.

Fig. 5.2 shows the self-organized state ($t = 20$), where an appreciable zonal component manifests. In Fig. 5.3, we compare the Fourier spectrum of the zonal component $\omega_z = \mathcal{P}_z\omega$ in the initial and self-organized states. We find the redistribution of the spectrum into lower λ modes (i.e., inverse cascade). A comparison with the Rhines scale will be described later.

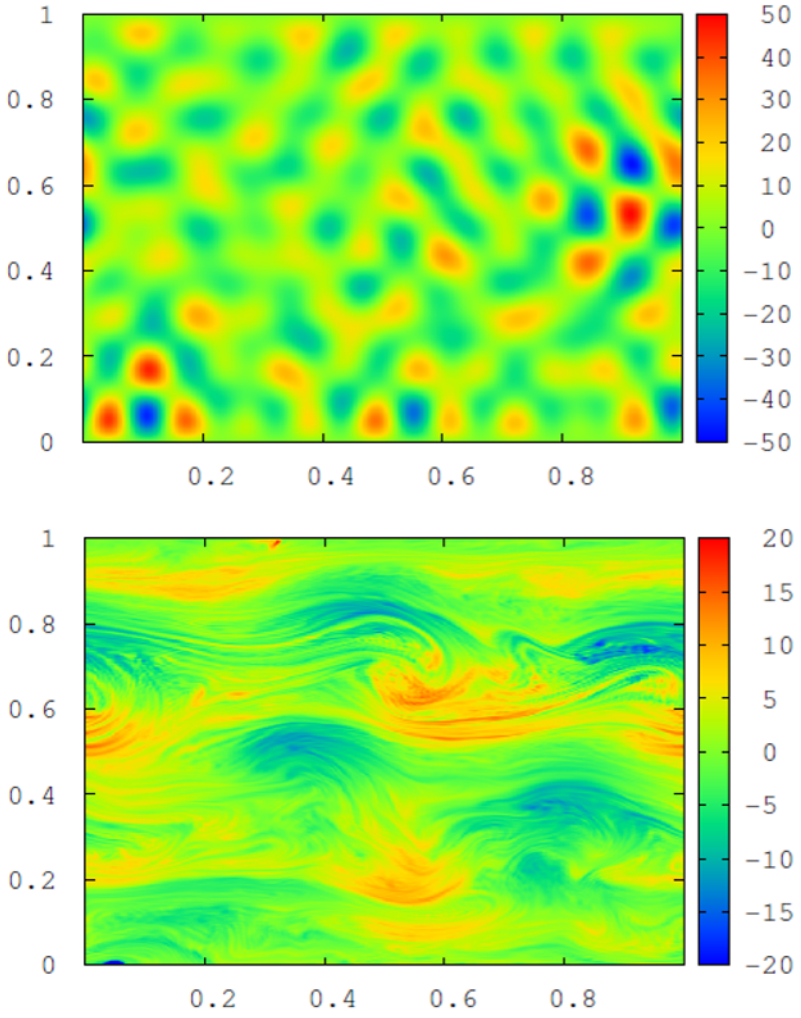

Figure 5.2: Self-organization of zonal flow (color map represents to the local value of ω). (left) Initial condition with finite circulation $C_F = 0.21$ and impulse $C_L = 0.11$. (right) Creation of zonal flow observed at $t = 20$.

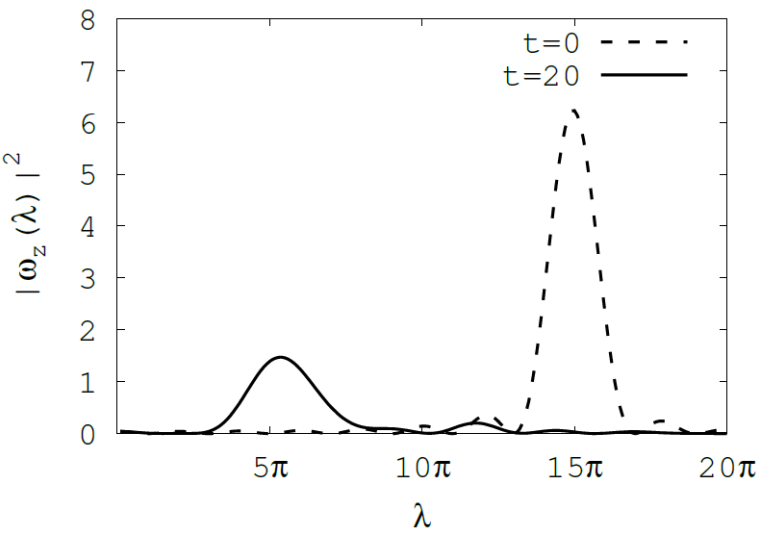

Figure 5.3: The Fourier spectrum of the zonal vorticity $\omega_z = \mathcal{P}_z\omega$ in the self-organized state ($t = 20$). The eigenvalue $\lambda \sim 5\pi$ is dominant.

To make comparison with the theoretical estimate of zonal enstrophy, we plot Z_λ (the theoretical minimum of zonal enstrophy) and $C_E\lambda^2$ (the theoretical maximum of zonal enstrophy), evaluated for the parameters determined by the given initial condition, in Fig. 5.4. As $\lambda = 5\pi$ is the dominant mode (Fig. 5.3), we obtain $Z_\lambda = 0.69$ and $C_E\lambda^2 = 8.8$. In Fig. 5.5, we compare the simulation result and the theoretical estimates, demonstrating that the actual zonal enstrophy $Z(\omega)$ stays between the theoretical minimum and maximum; the estimate of the lower bound is reasonably accurate.

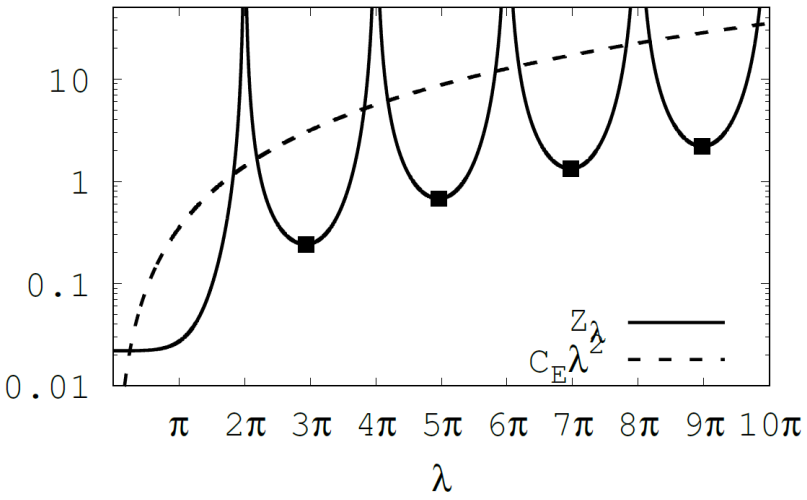

Figure 5.4: The graphs of Z_λ and $C_E\lambda^2$, evaluated for the parameters corresponding to the simulation of Fig. 5.2. The points on the curve indicates the eigenvalues.

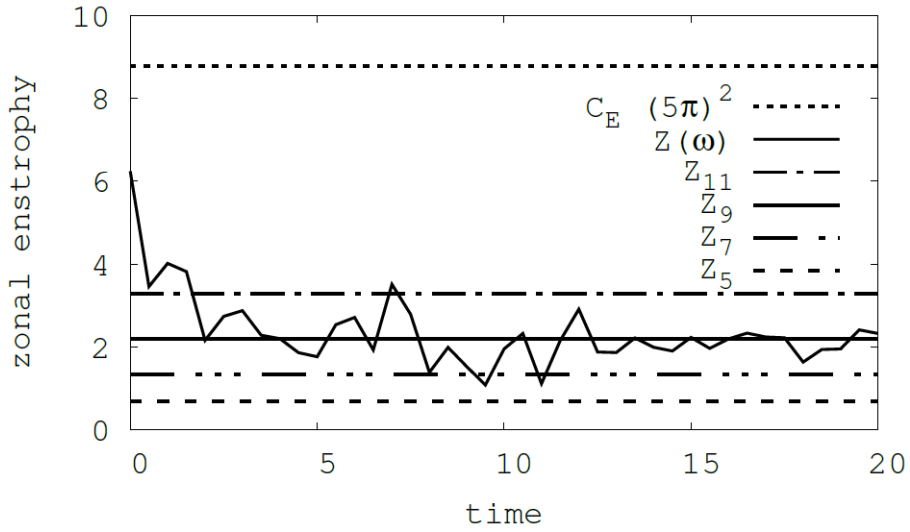

Figure 5.5: Evolution of the zonal enstrophy $Z(\omega)$, and its comparison with the theoretical minimum Z_λ and the maximum $C_E\lambda^2$ evaluated for the self-organized state $\lambda \sim 5\pi$. To demonstrate the sensitivity of the minimum value, we also show the theoretical minimum Z_λ evaluated for $\lambda \sim 5\pi$, 7π, 9π and 11π.

5.3 Improved Rhines scale

The forgoing discussion depends on the *a posteriori* estimate of the eigenvalue λ. As discussed in Sec. 4.5, however, we need an *a priori* estimate of λ to make the theory useful. While the Rhines scale L_R has been proposed to estimate $\lambda \sim \pi/L_R$, it turns out to be too crude. Here, we propose an improved Rhines scale to make more accurate estimate. Figure 5.6 compares the dominant scale in the final state obtained by simulation and the Rhines scale for different values of β. It is shown that the dominant scale is approximately 3 times of the Rhines scale.

The Rhines scale (4.49) is the length scale L_R at which the magnitudes of the nonlinear term $\{\omega, \psi\}$ and the linear term $\beta\{y, \psi\}$ become comparable. However, it seems that the function of the nonlinear term, that derives the relaxation of the enstrophy level λ, does not end immediately at L_R; the numerical experiment shows that the relaxation continues up to $\sim 3 \times L_R$, where the magnitude of the nonlinear term becomes about one eighth of the linear term. Therefore, we propose to use $L_R^* = 3L_R$ for the *a priori* estimate $\lambda = \pi/L_R^*$; modifying (4.50), we estimate

$$\lambda \sim \frac{\pi}{3}\sqrt{\frac{\beta}{2\sqrt{2C_E}}}. \tag{5.7}$$

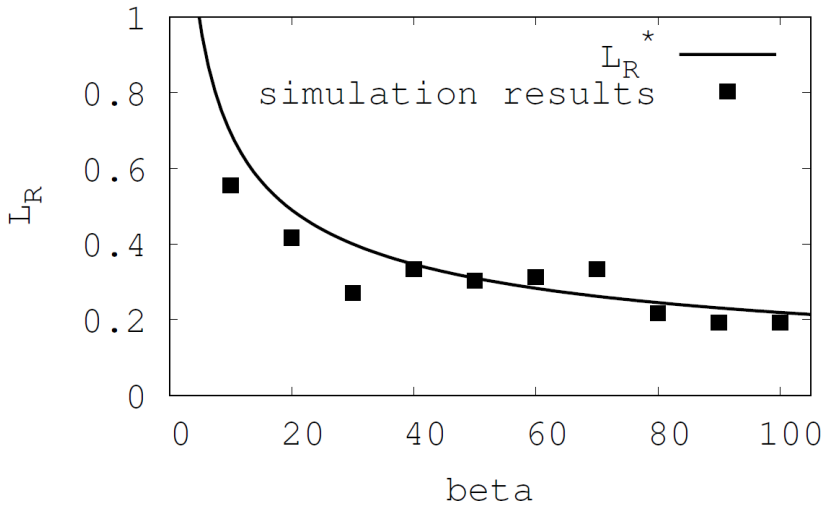

Figure 5.6: The comparison between the dominant scale in the self-organized state and the Rhines scale for different values of β. L_R^* denotes the modified Rhines scale.

5.4 Degenerate case: $C_F = 0$ and $C_L = 0$

Finally, we examine the degenerate case of $C_F = 0$ and $C_L = 0$, where we cannot provide nontrivial estimate of the minimum zonal enstrophy (see Theorem 2-2). However, we still observe self-organization of zonal flow, and the corresponding enstrophy satisfies the maximum condition.

Figure 5.7 shows the creation of zonal flow from an initial condition

$$\omega|_{t=0} = \sum_{m,n} \alpha_{mn} e^{imx} \sin n\pi y,$$

with random $\alpha_{mn}(|\alpha_{mn}| \in [0, 50)$ for $5 \le m, n \le 10)$ which is free from zonal component ($\omega_z = 0$ at $t = 0$). The symmetry also yields $C_F = 0$ and $C_L = 0$, so that the special condition of Theorem 2-2 applies. We only have a nontrivial estimate of the upper bound of $Z(\omega)$.

In Fig. 5.8, we plot the evolution of the zonal enstrophy $Z(\omega)$, and compare it with the theoretical maximum (4.27). Here we used $\lambda = 5\pi \sim 1/L_R^*$ by the improved Rhines estimate; in Fig. 5.9, we show the Fourier spectrum of ω_z, which supports the choice. We

observe that the time-asymptotic value of $Z(\omega)$ stays below the upper bound $C_E\lambda^2$.

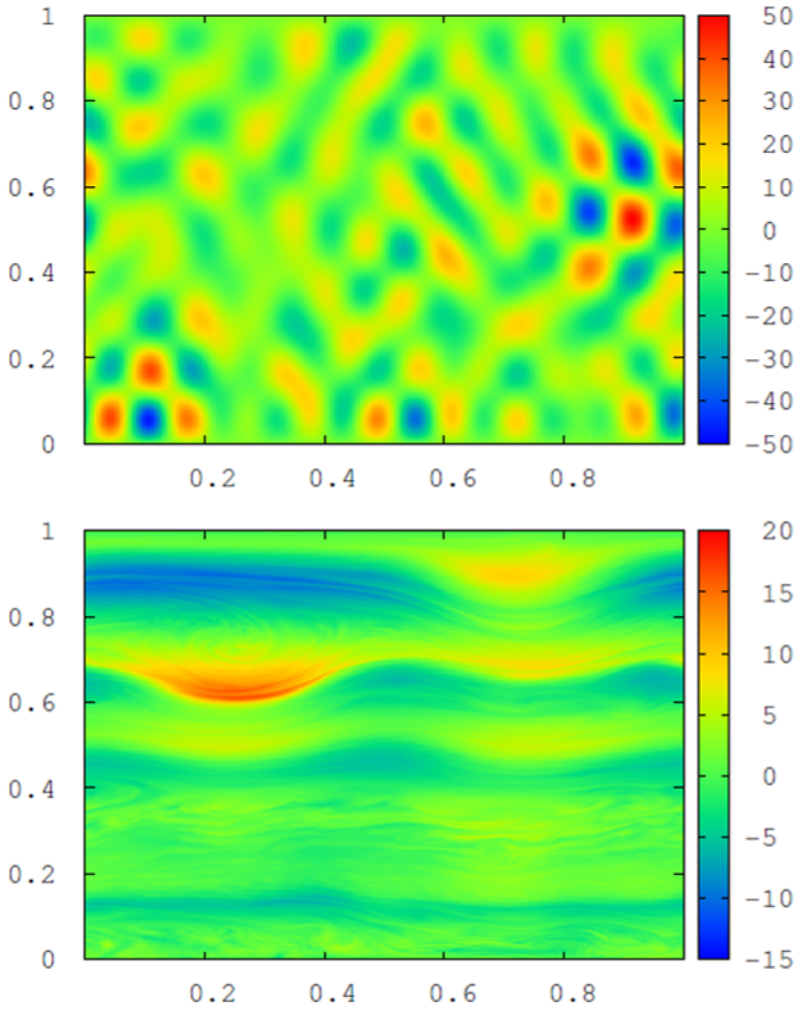

Figure 5.7: Self-organization of zonal flow (color map corresponds to the local value of ω). (left) Initial condition with zero zonal component $\omega_z = 0$. (right) Creation of zonal flow observed at $t = 50$.

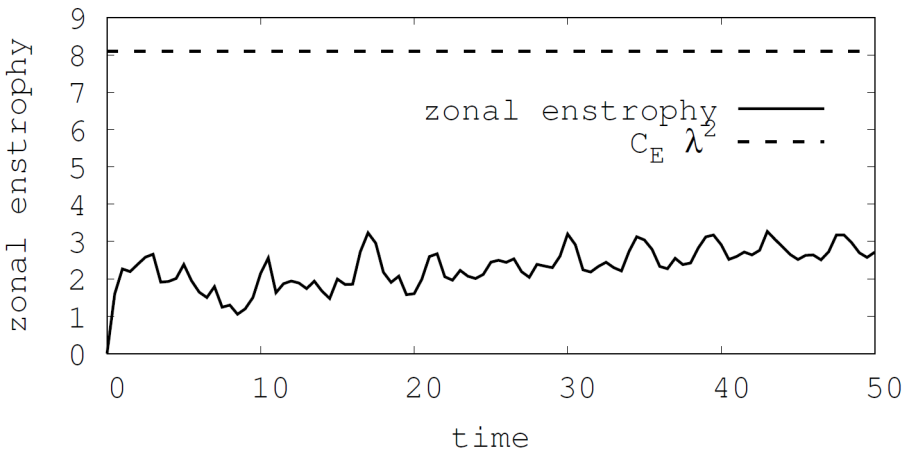

Figure 5.8: Evolution of the zonal enstrophy $Z(\omega)$ and its comparison with the theoretical estimate (upper bound).

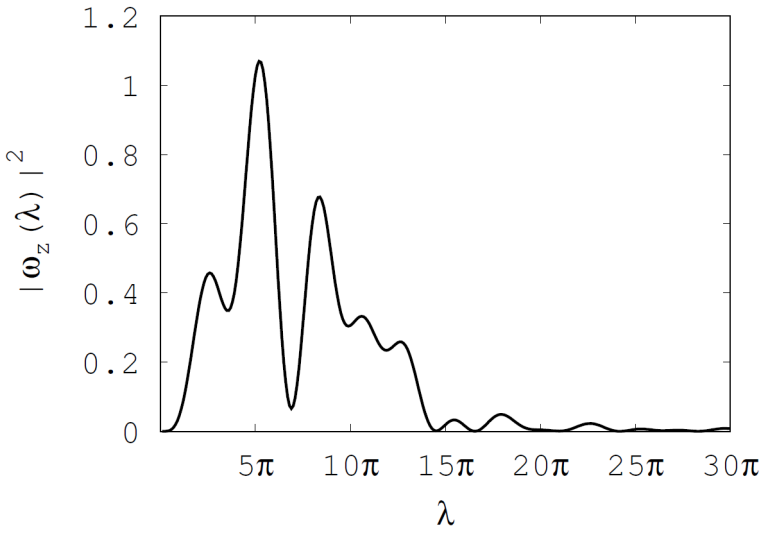

Figure 5.9: Fourier spectrum of the zonal vorticity in the self-organized state (Fig. 5.7 (right)).

Chapter 6

Conclusion of Part I

We have found a discrete set of *zonal enstrophy levels* that are quantized by the eigenvalue λ measuring the mode number (= system size in the latitude direction / lamination number). As shown in Fig.4.3, a finite circulation C_F and/or impulse C_L bring about symmetry breaking in the eigenstates (minimizers), inhibiting even mode numbers. In actual situation, however, the *mixed state* may include spectra of even mode numbers (see Figs. 5.3). By comparing with simulation results, we verified that the theoretical value Z_λ gives a reasonable estimate of the zonal enstrophy, if we choose the relevant mode number. We note that the enstrophy levels are determined independently of the selection mechanism. Just as the quantum energy level of an orbital electron is lowered by photon emission (see Fig. 6.1), the relaxation of the zonal enstrophy level proceeds by the emission of short-scale wavy vorticity. The relaxation process can be viewed as the forward cascade of enstrophy (creation of short-scale wavy vortices) and the simultaneous inverse cascade of the energy spectrum (deexcitation to lower zonal enstrophy states). The energy constraint plays an essential role in selecting the level; the relaxation continues as far as the nonlinear term, measured by the energy, dominates the evolution. The Rhines scale estimates the balance point of the magnitudes of the nonlinear term and the linear Rossby wave term, but we found that the nonlinear effect continues to work until it becomes about one order of magnitude smaller than the linear term, so we propose an improved Rhines scale.

Comparing Theorems 1 and 2, we find that the energy constraint $E(\omega) = C_E$ plays

an essential role in creating the discrete zonal enstrophy levels Z_λ. Interestingly, the value C_E does not influence the value of each zonal enstrophy Z_λ, which is determined only by the other constants C_F (circulation) and C_L (impulse). However, in absence of the energy constraint, we only have the "ground state" $\lambda = 0$ as given in Theorem 1. In the eigenstate of ω_z (belonging to the eigenvalue λ), the zonal enstrophy $Z(\omega_z)$ and the zonal energy $E(\omega_z)$ are related by $Z(\omega_z) = \lambda^2 E(\omega_z)$. Under the energy constraint (and a fixed λ), therefore, $Z(\omega_z)$ may take a smaller value when the wavy component ω_w shares a larger energy $E(\omega_w)$. The simultaneous total enstrophy constraint contributes to determining the wave number k of the wavy component ω_w. Without the symmetry breaking constraints by the circulation $F(\omega)$ and the impulse $L(\omega)$, $E(\omega_z)$ can minimize to zero (see Fig. 4.1), and then, $k \to \infty$ (independently of the specific value of C_Q). Finite symmetry breaking by C_F and/or C_L brings about a non-trivial minimum $E(\omega_z)$ (and the corresponding $Z(\omega_z) = \lambda^2 E(\omega_z)$). Then, the partition of the energy to the wavy component is determined as $E(\omega_w) = C_E - E(\omega_z)$, and the wave number k is determined by $k^2 E(\omega_w) = C_Q - Z(\omega_z)$. Interestingly, we may not remove the total enstrophy constraint from the variational principle, in order to retain a finite wavy component as the complementary to the zonal component, while its role is limited to characterizing only the wavy component. This unusual phenomenon in the variational principle is caused by the non-coerciveness of the target functional $Z(\omega)$ with respect to the norm $\|\omega\|$.

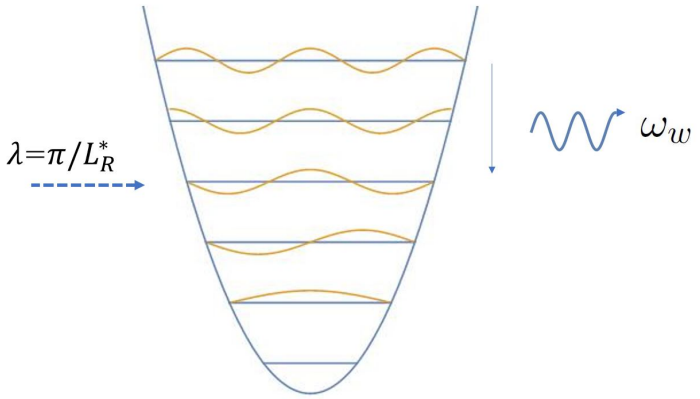

Figure 6.1: Analogy of quantum energy levels and "deexcitation" by emitting small-scale wavy enstrophy, which parallels the forward cascade of enstrophy.

Appendix of part I

A The ABC of variational principle

To see the mathematical non-triviality of the variational principle for the zonal enstrophy in Part I, we review the standard relation between the target functional and constraint.

A.1 Target functional and constraint

We start with a textbook example. The isoperimetric problem is to (1) maximize the surface area S with a constraint on the periphery length L, or (2) minimize the peripheral length L with a constraint on the surface area S. Both problems have the same solution, i.e. a circular disk or its periphery. Notice that reversing the target and constraint in each setting results in an *ill-posed* problem; one can make L infinitely long without changing S, or one can make S infinitely small without changing L. Let us concentrate on minimization problems. For a variational principle to be *well-posed*, the target (L) must be "fragile" and the constraint (S) must be robust. Here the fragility speaks of the sensitivity to small-scale perturbations. Suppose that we make pleats on a periphery; then L is increased, but S is not necessarily changed. In analytical formalism, a fragile functional includes a larger number of differentiations —derivatives are sensitive to small-scale perturbations. In the forgoing example, we may formally write

$$S = \int_{\mathbb{R}^2} \mathbb{I}_M \mathrm{d}^2 x, \quad L = \int_{\mathbb{R}^2} |\nabla \mathbb{I}_M| \mathrm{d}^2 x, \quad \mathbb{I}_M(\boldsymbol{x}) = \begin{cases} 1 & \text{if } \boldsymbol{x} \in M \\ 0 & \text{if } \boldsymbol{x} \notin M, \end{cases}$$

where M is a simply-connected domain $\subset \mathbb{R}^2$ that should be optimized to minimize L for some given value of S. Including ∇ in the integrand, L is fragile.

A.2 Coerciveness and continuity

To make the argument more precise, we introduce the notion of *coercive functionals*; cf. [37, 38]. Let u be a real-valued function (state vector) belonging to a function space (phase space) V, which is a Banach space with a norm $\|u\|$. A real-valued functional $G(u)$ is said coercive, if

$$\|u\|^2 \leq c\, G(u), \tag{A.1}$$

where c is some positive constant. On the other hand, a real-valued functional $H(u)$ is continuous, if

$$|H(u+\delta) - H(u)| \to 0 \quad (\|\delta\| \to 0). \tag{A.2}$$

We can formulate a well-posed minimization problem with a coercive target functional $G(u)$ and a continuous constraining functional $H(u)$ (we may also consider multiple constraints with continuous functionals).

To see how the coerciveness and continuity influence variational principles, let us consider an example with two functionals

$$G(u) = \int_M |\nabla u(\boldsymbol{x})|^2 \mathrm{d}^n x, \quad H(u) = \int_M |u(\boldsymbol{x})|^2 \mathrm{d}^n x,$$

where u is a scalar function defined in a smoothly bounded open set $M \subset \mathbb{R}^n$. We assume that $u = 0$ on the boundary ∂M. Notice that $H(u)^{1/2}$ is the L^2 norm $\|u\|$. Therefore, $H(u)$ is a continuous functional on the function space $V = L^2(M)$. By the Poincaré inequality, we have

$$\|u\|^2 \leq c\|\nabla u\|^2 = cG(u)$$

with a positive constant c. Therefore, $G(u)$ is a coercive functional.

First, we seek for a minimizer of $G(u)$ with the constraint $H(u) = 1$. This is a well-posed problem. The minimizer is found by the variational principle

$$\delta[G(u) - \lambda H(u)] = 0, \tag{A.3}$$

where λ is a Lagrange multiplier. The Euler-Lagrange equation

$$-\Delta u = \lambda u,$$

together with the above-mentioned boundary condition, constitute an eigenvalue problem. We can easily show that every eigenvalue λ is positive. Let λ_j be an eigenvalue and φ_j be the corresponding normalized eigenfunction ($\|\varphi_j\|^2 = 1$). With setting $u = a\varphi_j$, and demanding $H(u) = 1$, we obtain $a = 1$ and $G(u) = \lambda_j$. The smallest λ_j, then, yields the minimum $G(u)$.

The reversed problem of finding a minimizer of $H(u)$ with the restriction $G(u) = 1$ is ill-posed, because the constraint is posed by a functional $G(u)$ that is not continuous in the topology of $L^2(M)$. Let us elucidate the pathology. The variational principle $\delta[H(u) - \mu G(u)] = 0$ (μ is a Lagrange multiplier) yields the Euler-Lagrange equation $-\Delta u = \mu^{-1} u$. Let $\mu^{-1} = \lambda_j$ (an eigenvalue of $-\Delta$), and $u = a\varphi_j$. The condition $G(u) = 1$ yields $a = \lambda_j^{-1/2}$, and $H(u) = 1/\lambda_j$. Hence, the minimum of $H(u)$ is achieved by the largest eigenvalue that is unbounded, viz., $\inf H(u) = 0$ and the minimizer $\lim_{\lambda_j \to \infty} \lambda_j^{-1/2} \varphi_j = 0$ is nothing but the minimizer of $H(u)$ without any restriction. The constraint $G(u) = 1$ plays no role in this minimization problem.

A.3 Non-coercive target functional

Let us modify the target functional of (A.3) to a non-coercive functional. Let $V_k = \mathrm{span}\,\{\varphi_1, \cdots, \varphi_k\}$, which is a closed (finite-dimension) subspace of $V = L^2(M)$. We denote the orthogonal complement by V', i.e. we decompose $V = V_k \oplus V'$. Let $\mathcal{P}$ be the orthogonal projector $V \to V'$. Consider

$$G'(u) = \|\nabla(\mathcal{P}u)\|^2 = \int_M (-\Delta \mathcal{P}u)(\mathcal{P}u)\,\mathrm{d}^n x = \sum_{j>k}^{\infty} \lambda_j (u, \varphi_j)^2,$$

where $(f, g) = \int_M f(\boldsymbol{x})\, g(\boldsymbol{x})\,\mathrm{d}^n x$ is the inner product of $L^2(M)$. Evidently, $G'(u)$ is not coercive. The modified variational principle

$$\delta[G'(u) - \lambda H(u)] = 0 \tag{A.4}$$

yields the Euler-Lagrange equation that reads, after expanding with eigenfunctions,

$$\lambda'_j(u, \varphi_j) = \lambda(u, \varphi_j) \quad (j = 1, 2, \cdots), \tag{A.5}$$

where the "modified eigenvalues" are

$$\lambda'_j = \begin{cases} 0 & (j = 1, \cdots, k), \\ \lambda_j & (j > k). \end{cases}$$

The minimizer of $G'(u)$ is a solution of (A.5) such that $\lambda = 0$ and

$$u = \sum_{j=1}^{k} a_j \varphi_j,$$

where constants $a_1, \cdots, a_k$ can be arbitrarily chosen provided that $\sum_{j=1}^{k} |a_j|^2 = 1$ in order to satisfy the constraint $H(u) = 1$. We obtain $\min G' = 0$, but the minimizer is not a unique function.

This prototypical example elucidates the essence of the pathology created in a variational principle with non-coercive target functional. We encounter a similar non-uniqueness (degeneracy) problem in Sec. 4.1. Interestingly, however, the energy constraint brings about a dramatic change in the mathematical structure, and removes the degeneracy; Sec. 4.3.

Part II

Kinetic construction of the high-beta anisotropic-pressure equilibrium in magnetosphere

Chapter 7

Introduction of Part II

7.1 Background and purpose of part II

The magnetosphere is a naturally made system confining a high-beta plasma [39]. A similar system may be created for fusion energy applications [40, 41]. Laboratory magnetospheres, namely, LDX [42] and RT-1 [43], demonstrated a stable confinement of high-beta (~ 1) plasmas.

The aim of this study is to formulate a theoretical model of high-beta equilibrium in the magnetosphere. Magnetized particles in an axisymmetric magnetic field have three independent first integrals, facilitating an easy construction of the equilibrium solutions of the drift kinetic equation. The strong inhomogeneity of the dipole magnetic field is the key to understanding the localization of magnetized particles to the vicinity of the magnetic dipole [40]. However, in a high-beta plasma, the magnetic field must be corrected by considering the diamagnetic current. We observe a significant expansion of the dipole field due to plasma pressure, which can be used to estimate the plasma pressure [44, 45]. At the first-order level, we may invoke the Grad–Shafranov equation [46] to analyze the magnetic field of a finite-beta plasma. However, this equation falls short of considering the strong anisotropy of the distribution function, as the kinetic model makes predictions for the magnetospheric system. The bounce of mirror-trapped particles introduces variations in the velocity distribution function along the field lines. The anisotropic temperature is also demonstrated experimentally in RT-1 [47]. Appropriate corrections can be made by using

the extended Grad–Shafranov equation, which was developed to model the equilibrium of mirror systems [48, 49]. In fact, each magnetic flux tube in the magnetosphere may be viewed as a crescent-shaped mirror system. The extended Grad–Shafranov equation, which is still a macroscopic magneto-fluid model, considers an anisotropic pressure that is a function of the two-dimensional magnetic coordinates, namely, the flux function and magnetic field strength. While the functional form of the pressure tensor remains arbitrary in such a fluid model, parametric studies on the effect of anisotropic pressure have been performed using numerical analysis [50, 51]. We have yet to build a consistent relationship between the kinetic description and the magneto-fluid model, and to provide a physical reason for selecting an appropriate form of the pressure tensor.

In the present study, we constructed a self-consistent model based on the idea of the maximum entropy state in a topologically constrained phase space (or a symplectic leaf foliated by Casimirs) [52]. In the context of magnetospheric plasma confinement, the adiabatic invariant acts as a topological constraint (Casimir of the noncanonical Hamiltonian mechanics [34]). Providing the topological charge (in fact, the Casimir) with a chemical potential, we define a grand canonical ensemble, on which we consider the Gibbs distribution. As the magnetic moment is the relevant Casimir, the pair of chemical potential and Casimir parallels that of the magnetic field and magnetization in the well-known model of magnetic materials. Such a "thermal equilibrium" yields the desired pressure tensor to be used in the generalized Grad–Shafranov equation.

7.2 Outline of part II

Part II is organized as follows: In the following chapter, we review the Hamiltonian mechanics of magnetized particles and derive the stationary distribution function that describes the thermal equilibrium under the topological constraint given by the magnetization. The corresponding pressure tensor is used to formulate the generalized (anisotropic pressure) Grad–Shafranov equation in chapter 9. In chapter 10, we show examples of numerical solutions, as well as some relations useful to estimate the anisotropic pressure effect. Chapter 11 concludes part II.

Chapter 8

Theoretical model

To construct the high-beta equilibrium of magnetospheric plasma, we combine two models: one is the kinetic model for calculating the distribution function, and the other is the macroscopic magneto-fluid magnetohydrodynamics (MHD) model for calculating the magnetic field. The distribution function is given as a stationary solution of the Vlasov theory with appropriate coarse graining. Evaluating the pressure tensor using the distribution function, we solve the generalized (anisotropic pressure) Grad–Shafranov equation to determine the magnetic field.

8.1 Hamiltonian of magnetized particles in magnetosphere

In an axisymmetric magnetic field (of sufficient strength), the dynamics of a magnetized particle consist of three different periodic motions: gyro motion, bounce motion, and drift motion. It is then convenient to span the phase space by variables

$$\boldsymbol{z} = (\theta_g,\, \mu,\, ;\, \ell,\, P_\parallel\, ;\, \theta,\, P_\theta), \tag{8.1}$$

where $\mu := J_g q/m$ is the magnetic moment (J_g is the action corresponding to the gyro motion, q is the particle charge, and m is the particle mass), θ_g is the gyro angle, $P_\parallel$ is the canonical momentum parallel to the magnetic field, ℓ is the parallel coordinate that constitutes the canonical pair with $P_\parallel$, P_θ is the canonical angular momentum around the geometrical axis, and θ is the azimuthal angle. (For convenience, we use ℓ, $P_\parallel$, instead

of the bounce action-angle pair). Neglecting the kinetic part of the canonical angular momentum, we approximate $P_\theta = q\psi$ ($\psi = rA_\theta$ is the flux function in the cylindrical coordinate system (r, θ, z), where A_θ is the θ component of the vector potential).

Here, we consider two different "reductions" for the Hamiltonian. First, the gyro angle θ_g is *coarse-grained* and is eliminated from the Hamiltonian (such a Hamiltonian only dictates the guiding center motion of the magnetized particle). Then, we obtain

$$\dot{\mu} = \frac{\partial H}{\partial \theta_g} = 0. \tag{8.2}$$

Second, we assume axisymmetry so that the Hamiltonian is independent of the azimuthal angle θ. With the approximation $P_\theta = q\psi$, we obtain

$$q\dot{\psi} = \dot{P}_\theta = \frac{\partial H}{\partial \theta} = 0. \tag{8.3}$$

The two constants μ and ψ play an important role in later discussion.

The magnetic field may be written as $\boldsymbol{B} = \nabla\psi \times \nabla\theta$ (note that the toroidal magnetic field is absent in the magnetospheric system). By adding the coordinate ℓ that measures the arch length on each magnetic field line, we define a magnetic coordinate system (ℓ, ψ, θ). Through the axisymmetry, we can eliminate θ.

8.2 Kinetic distribution function

8.2.1 General form of stationary distribution function

In the Vlasov theory, the stationary distribution function f is given by

$$\{H, f^*\} = 0, \tag{8.4}$$

where $\{\ ,\ \}$ is the canonical Poisson bracket, and f^* is the Hodge dual of f, i.e., $f = f^*\mathrm{vol}$ with the phase-space volume element $\mathrm{vol} = \mathrm{d}^3x\mathrm{d}^3v$. When $\{G_j, H\} = 0$, G_j is a constant of motion. A scalar function such as $f^*(H, G_1, \cdots, G_n)$ gives a stationary distribution

$f = f^*\text{vol}$, because

$$\{H, f^*(H, G_1, \cdots, G_n)\} = \frac{\partial f^*}{\partial H}\{H, H\} + \sum_{j=1}^{m} \frac{\partial f^*}{\partial G_j}\{G_j, H\} = 0.$$

Here, we use the aforementioned μ and ψ to define a stationary distribution function using

$$f^* = g(H, \mu, \psi), \tag{8.5}$$

where g is an arbitrary function of H, μ, and ψ.

8.2.2 Thermal equilibrium with topological constraints

Although the collisionless kinetic theory leaves infinite freedom in the stationary distribution function, it provides us with the theoretical basis for statistical mechanics to define the most probable distribution with the appropriately defined entropy, that is, the invariant measure is determined by the guide of the Poisson structure pertinent to the kinetic theory. Here, the invariant measure is given on the symplectic leaf, defined as the level sets of the two invariants μ and ψ.

We consider the Hamiltonian

$$H = \mu B(\ell, \psi) + \frac{P_\parallel^2}{2m}, \tag{8.6}$$

where B is the magnetic field. Here, we consider a quasi-neutral plasma ($\phi = 0$) and neglect the kinetic energy of the toroidal drift velocity by approximating $P_\theta = q\psi$. The first term μB may be regarded as the potential energy (μ is constant for each particle) on each contour of ψ (i.e., magnetic field line).

Leaving only ψ as a free parameter characterizing the thermal nonequilibrium of the system, we consider the thermal equilibrium (maximum entropy) distribution function such that (see Appendix B)

$$f^* = A(\psi) \exp\left(-\frac{H}{T_{\parallel 0}}\right) \exp\left(-\mu B_0(\psi) \frac{T_{\parallel 0} - T_{\perp 0}}{T_{\parallel 0} T_{\perp 0}}\right), \tag{8.7}$$

where the two constants $T_{\parallel 0}$ and $T_{\perp 0}$ represent the parallel and perpendicular temperatures

at $\ell = 0$, respectively. We also define $B_0(\psi) := B(0, \psi)$, where $B(\ell, \psi)$ is the magnetic field strength evaluated as a function of ℓ and ψ.

Then, by substituting (8.6) and $\mu = \dfrac{mv_\perp^2}{2B(\ell, \psi)}$ in (8.7), we can rewrite (8.7) as

$$f^* = A(\psi) \exp\left\{ -\left(\frac{mv_\parallel^2}{2T_\parallel(\ell, \psi)} + \frac{mv_\perp^2}{2T_\perp(\ell, \psi)} \right) \right\}, \tag{8.8}$$

where

$$T_\parallel(\ell, \psi) = T_{\parallel 0}, \tag{8.9}$$

$$T_\perp(\ell, \psi) = \frac{T_{\parallel 0} T_{\perp 0}}{T_{\perp 0} + \frac{B_0(\psi)}{B(\ell, \psi)}(T_{\parallel 0} - T_{\perp 0})}. \tag{8.10}$$

Therefore, our distribution function is a Maxwellian with varying anisotropic temperatures (8.9) and (8.10). Multiplying the phase-space volume form, we obtain

$$f = f^* \mathrm{d}^3x \, \mathrm{d}^3v \tag{8.11}$$

$$= f^* \mathrm{d}^3x \, \frac{D(v_x, v_y, v_z)}{D(v_\parallel, v_\perp, \theta_g)} \mathrm{d}v_\parallel \mathrm{d}v_\perp \mathrm{d}\theta_g \tag{8.12}$$

$$= v_\perp A(\psi) \exp\left\{ -\left(\frac{mv_\parallel^2}{2T_\parallel(\ell, \psi)} + \frac{mv_\perp^2}{2T_\perp(\ell, \psi)} \right) \right\} \mathrm{d}^3x \, \mathrm{d}v_\parallel \mathrm{d}v_\perp \mathrm{d}\theta_g. \tag{8.13}$$

Transforming variables in the volume form, we rewrite

$$f(\ell, \psi, v_\parallel, v_\perp) = 2\pi v_\perp A(\psi) \exp\left\{ -\left(\frac{mv_\parallel^2}{2T_\parallel(\ell, \psi)} + \frac{mv_\perp^2}{2T_\perp(\ell, \psi)} \right) \right\} \mathrm{d}^3x \, \mathrm{d}v_\parallel \mathrm{d}v_\perp. \tag{8.14}$$

The corresponding configuration space density is

$$n(\ell, \psi) = \iint f(\ell, \psi, v_\parallel, v_\perp) \, \mathrm{d}v_\parallel \mathrm{d}v_\perp \tag{8.15}$$

$$= A(\psi) \left(\frac{2\pi}{m} \right)^{\frac{3}{2}} T_\parallel^{\frac{1}{2}}(\ell, \psi) \, T_\perp(\ell, \psi), \tag{8.16}$$

and the parallel and perpendicular components of the pressure tensor are

$$p_{\parallel}(\ell,\psi) = \iint f(\ell,\psi,v_{\parallel},v_{\perp})\, m v_{\parallel}^2 \mathrm{d}v_{\parallel}\mathrm{d}v_{\perp} \tag{8.17}$$

$$= A(\psi)\left(\frac{2\pi}{m}\right)^{\frac{3}{2}} T_{\parallel}^{\frac{3}{2}}(\ell,\psi) T_{\perp}(\ell,\psi), \tag{8.18}$$

$$p_{\perp}(\ell,\psi) = \frac{1}{2}\iint f(\ell,\psi,v_{\parallel},v_{\perp})\, m v_{\perp}^2 \mathrm{d}v_{\parallel}\mathrm{d}v_{\perp} \tag{8.19}$$

$$= A(\psi)\left(\frac{2\pi}{m}\right)^{\frac{3}{2}} T_{\parallel}^{\frac{1}{2}}(\ell,\psi)\{T_{\perp}(\ell,\psi)\}^2. \tag{8.20}$$

Finally, we represent the pressures and functions of the magnetic coordinates ψ and B, and using (8.9) and (8.10), we obtain

$$p_{\parallel}(\psi,B) = A(\psi)\left(\frac{2\pi}{m}\right)^{\frac{3}{2}} T_{\parallel 0}^{\frac{5}{2}} \frac{T_{\perp 0}}{T_{\perp 0} + \frac{B_0(\psi)}{B}(T_{\parallel 0} - T_{\perp 0})}, \tag{8.21}$$

$$p_{\perp}(\psi,B) = A(\psi)\left(\frac{2\pi}{m}\right)^{\frac{3}{2}} T_{\parallel 0}^{\frac{5}{2}} \left(\frac{T_{\perp 0}}{T_{\perp 0} + \frac{B_0(\psi)}{B}(T_{\parallel 0} - T_{\perp 0})}\right)^2. \tag{8.22}$$

Chapter 9

Finite-beta magnetic field

The anisotropic pressures (8.21) and (8.22), evaluated for the thermal equilibrium on the symplectic leaf of the magnetic moment, can now be used in the generalized Grad–Shafranov equation. The pressure tensor is

$$\mathbf{P} = \boldsymbol{bb}p_{\parallel} + (\mathbf{I} - \boldsymbol{bb})p_{\perp} \tag{9.1}$$

where $p_{\parallel}$ and $p_{\perp}$ are the parallel and perpendicular pressures, respectively, and $\boldsymbol{b}$ is the unit vector parallel to $\boldsymbol{B}$. The MHD equilibrium equations are

$$\nabla \times \boldsymbol{B} \times \boldsymbol{B} = \mu_0 \nabla \cdot \mathbf{P}, \tag{9.2}$$

$$\nabla \cdot \boldsymbol{B} = 0, \tag{9.3}$$

where μ_0 is the vacuum permeability. In the axisymmetric magnetospheric system (which has no toroidal magnetic field), we can convert the MHD equilibrium equation into a generalized (anisotropic pressure) Grad–Shafranov equation [48, 49]:

$$\Delta^* \psi = -\mu_0 r^2 \left.\frac{\partial p_{\parallel}}{\partial \psi}\right|_B - \frac{1}{\sigma} \nabla\psi \cdot \nabla\sigma \tag{9.4}$$

$$\left.\frac{\partial p_{\parallel}}{\partial B}\right|_{\psi} + \frac{p_{\perp} - p_{\parallel}}{B} = 0, \tag{9.5}$$

where Δ^* denotes the Grad–Shafranov operator

$$\Delta^* := r^2 \nabla \cdot (\frac{1}{r^2} \nabla), \tag{9.6}$$

and σ is defined as

$$\sigma := 1 + \mu_0 \frac{p_\perp - p_\parallel}{B^2}. \tag{9.7}$$

Note that (8.21) and (8.22) satisfy the second equation (9.5). We only need to solve (9.4) to determine ψ.

Chapter 10

Numerical analysis

In this chapter, we show the results of the numerical analysis conducted based on a numerical code RTEQ (Ring Trap EQuilibrium) developed by Furukawa [51].

10.1 Setting and calculation model

As we assume axisymmetry, we consider the 2D-plane shown in fig. 10.1. The magnetic field lines correspond to the ψ contour, and $l = 0$ on the magnetic field lines corresponds to the point where $z = 0$ at the outer side of the ring current. Here, ψ_1 and ψ_2 denote the magnetic field line that comes in contact with the fixed limiters that provide the boundary of the plasma. The inertial ring current generates the vacuum magnetic field.

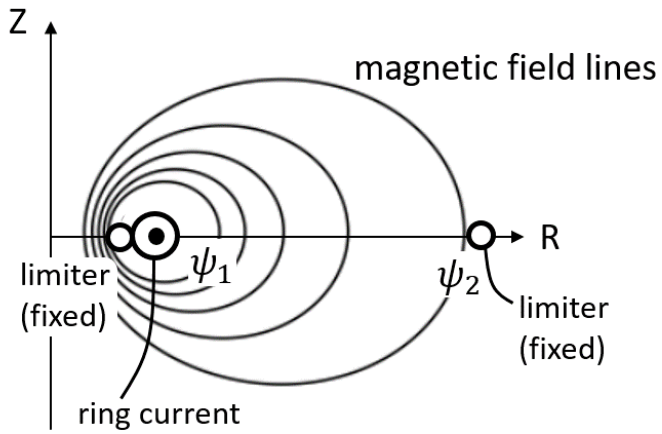

Figure 10.1: Schematic of the 2D-plane considered in the calculation

Normalized with the typical length L_1, magnetic field B_1, pressure p_1, and magnetic flux $\Psi_1 := B_1 L_1^2$, the Grad–Shafranov equation is expressed as follows:

$$\check{\Delta}^* \check{\psi} = -\frac{\beta_o}{2} \check{r}^2 \left. \frac{\partial \check{p}_{\parallel}}{\partial \check{\psi}} \right|_{\check{B}} - \frac{1}{\check{\sigma}} \check{\nabla} \check{\psi} \cdot \check{\nabla} \check{\sigma}, \tag{10.1}$$

where we apply (8.21) and (8.22) as the parallel and perpendicular components of the pressure tensor, respectively, which are rewritten as

$$\check{p}_{\parallel}(\psi,\, B) = \bar{p}(\check{\psi}) \frac{\lambda_0}{\lambda_0 + \frac{\check{B}_0(\psi)}{\check{B}}(1-\lambda_0)}, \tag{10.2}$$

$$\check{p}_{\perp}(\psi,\, B) = \bar{p}(\check{\psi}) \left(\frac{\lambda_0}{\lambda_0 + \frac{\check{B}_0(\psi)}{\check{B}}(1-\lambda_0)} \right)^2. \tag{10.3}$$

The boundary condition is $\psi = 0$ at infinity. The equation contains two parameters: $\beta_o := \dfrac{2\mu_0 p_1}{B_1^2}$ and $\lambda_0 := \dfrac{T_{\perp 0}}{T_{\parallel 0}}$. Here, λ_0 represents the temperature anisotropy on $l = 0$. Moreover, $\bar{p}(\check{\psi})$ corresponds to the normalized pressure in the isotropic case, which allows arbitrary functions of $\check{\psi}$. Here, we assume

$$\bar{p}(\check{\psi}) \propto -(\check{\psi} - \check{\psi}_1)^P (\check{\psi} - \check{\psi}_2)^Q. \tag{10.4}$$

Although we can treat P and Q as parameters, we fix $P = 1, Q = 1$ in this study for simplicity. Then, we obtain

$$\bar{p}(\check{\psi}) := -\frac{4(\check{\psi} - \check{\psi}_1)(\check{\psi} - \check{\psi}_2)}{(\check{\psi}_2 - \check{\psi}_1)^2}. \tag{10.5}$$

10.2 Effects of anisotropic temperature on the equilibrium states

First, we analyze the cases where $\lambda_0 \geq 1$. We show the distributions of $p_\parallel$ and $p_\perp$ in fig. 10.2 and those of ψ_p and β in fig. 10.3, which correspond to the equilibrium states calculated for $\beta_o = 4.5 \times 10^{-5}$ and (top) $\lambda_0 = 1.0$, (middle) $\lambda_0 = 1.5$, (bottom) $\lambda_0 = 2.0$. Here, $\beta := \dfrac{2\mu_0 p}{B^2}$ and $\psi_p := \psi - \psi_v$, where ψ_v denotes ψ, which corresponds to a vacuum magnetic field. As shown in fig. 10.2 when $\lambda_0 = 1$, the distributions of pressure become isotropic ($\check{p}_\parallel = \check{p}_\perp = p(\bar{\psi})$). Therefore, $p_\parallel$ and $p_\perp$ are constant along the magnetic field lines. On the other hand, when $\lambda_0 > 1$, $p_\parallel$ and $p_\perp$ are higher at the outer side of the ring current near $z = 0$. Moreover, as λ_0 increases, the distributions are more concentrated at the outer side of the ring current near $z = 0$, and the maximum local values of $p_\parallel$ and $p_\perp$ become higher. Even for ψ_p and β, the distributions are more concentrated at the outer side of the ring current near $z = 0$, and the maximum local values become higher as λ_0 increases; see fig. 10.3.

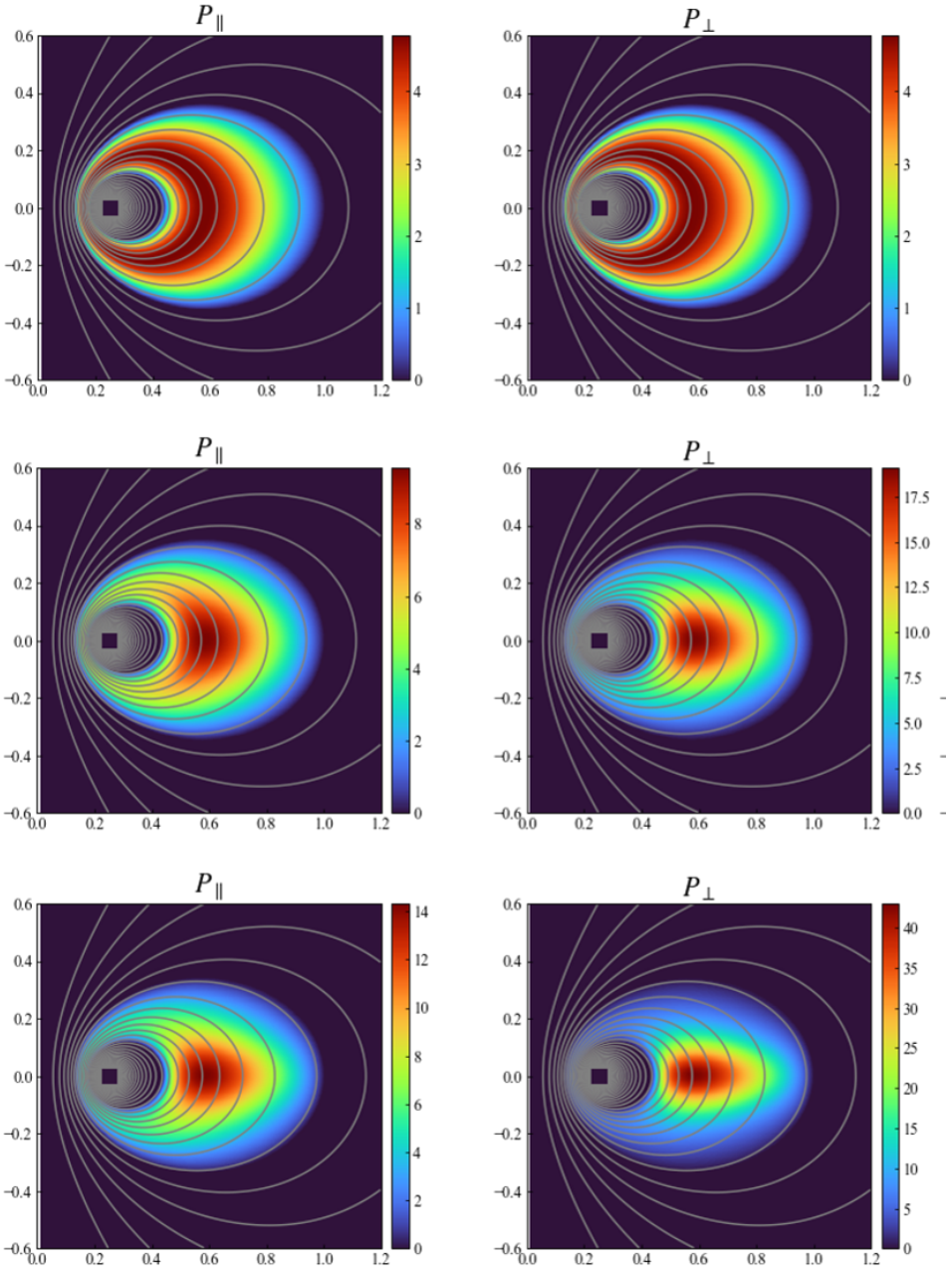

Figure 10.2: Distributions of $p_{\parallel}$ and $p_{\perp}$, which correspond to the equilibrium states calculated for $\beta_o = 4.5 \times 10^{-5}$ and (top) $\lambda_0 = 1.0$, (middle) $\lambda_0 = 1.5$, (bottom) $\lambda_0 = 2.0$

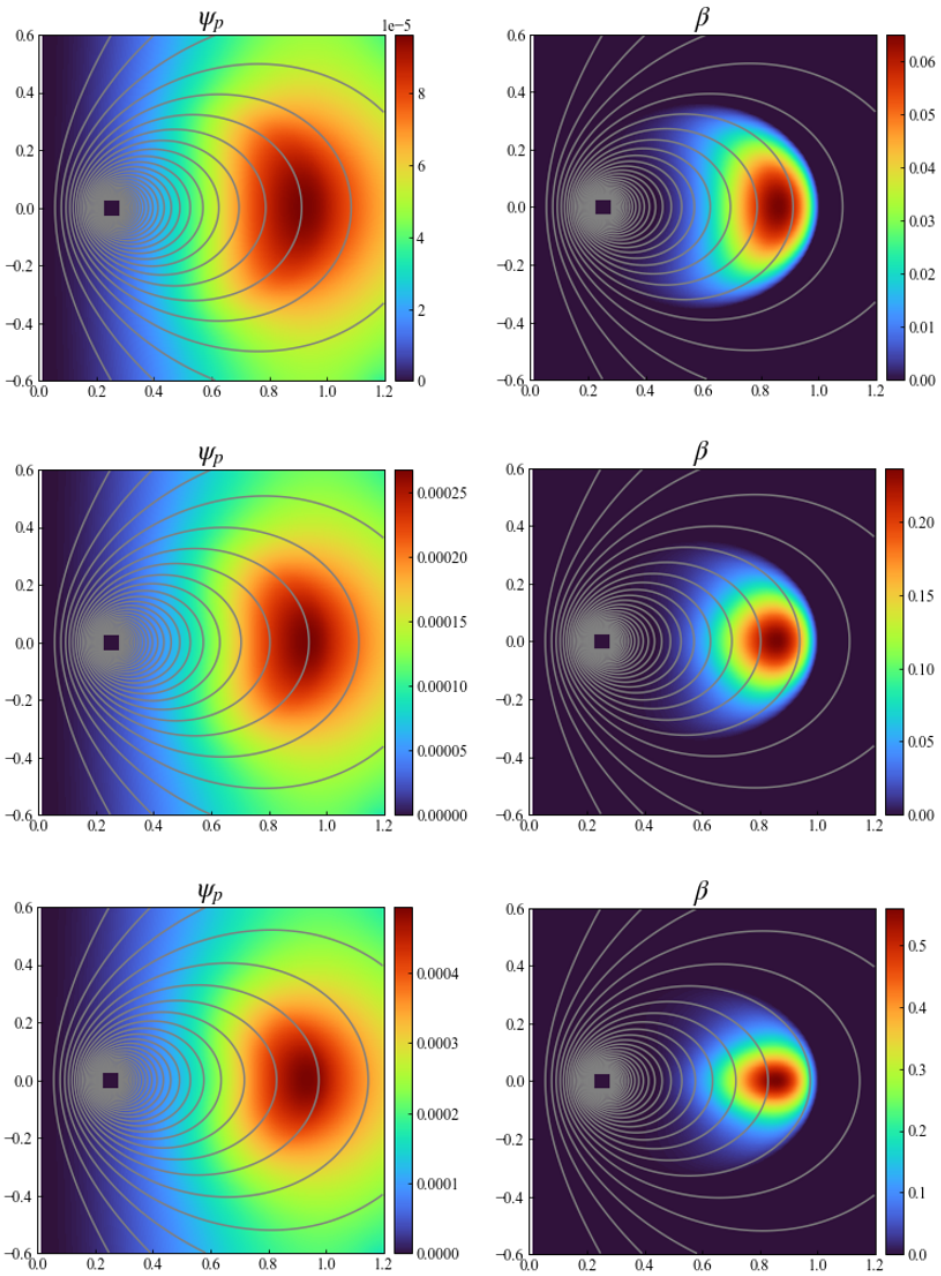

Figure 10.3: Distributions of ψ_p and β, which correspond to the equilibrium states calculated for $\beta_o = 4.5 \times 10^{-5}$ and (top) $\lambda_0 = 1.0$, (middle) $\lambda_0 = 1.5$, (bottom) $\lambda_0 = 2.0$

Next, we analyze the cases where $\lambda_0 < 1$. We show the distributions of $p_{\parallel}$ and $p_{\perp}$ in fig. 10.4 and those of ψ_p and β in fig. 10.5, which correspond to the equilibrium states calculated for $\beta_o = 4.5 \times 10^{-5}$ and (top) $\lambda_0 = 0.50$, (bottom) $\lambda_0 = 0.25$. In line with the

cases in which $\lambda \geq 1$, $p_{\|}$ and $p_{\perp}$ are higher at the inner side of the ring current near $z = 0$. Moreover, as λ_0 becomes smaller, the distributions are more concentrated at the inner side of the ring current near $z = 0$, but the maximum local values of $p_{\|}$ and $p_{\perp}$ become lower (see fig. 10.4). Regarding ψ_p and β, the distributions are concentrated at the outer side of the ring current, and the maximum local values become lower as λ_0 becomes smaller; see fig. 10.5.

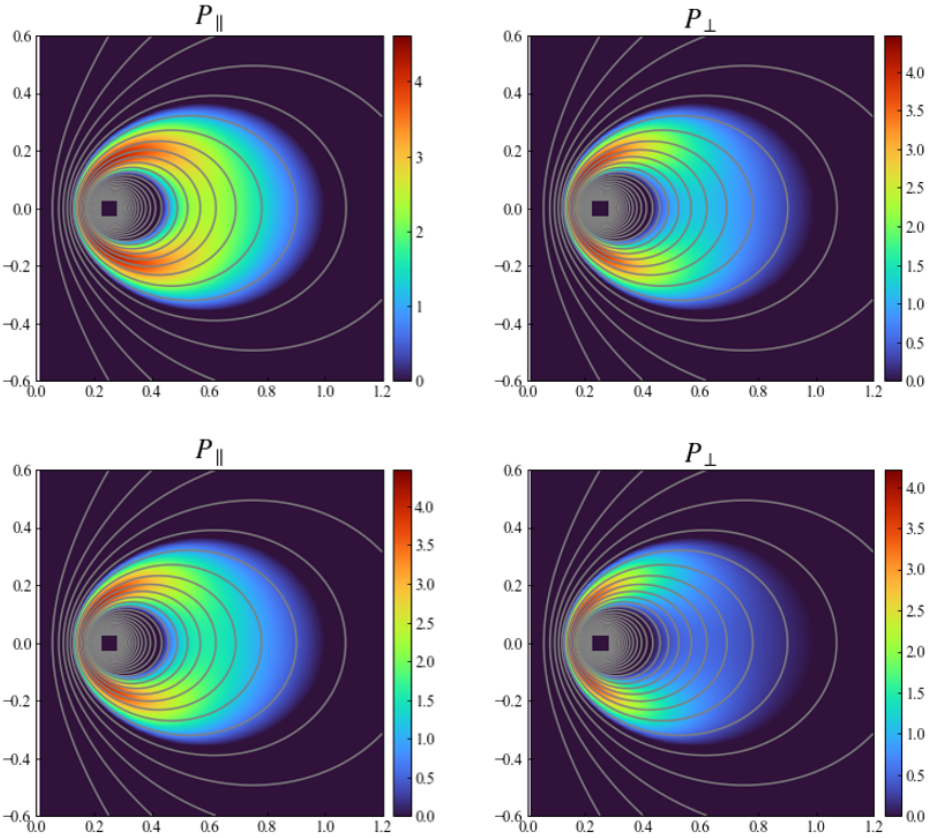

Figure 10.4: Distributions of $p_{\|}$ and $p_{\perp}$, which correspond to the equilibrium states calculated for $\beta_o = 4.5 \times 10^{-5}$ and (top) $\lambda_0 = 0.50$, (bottom) $\lambda_0 = 0.25$

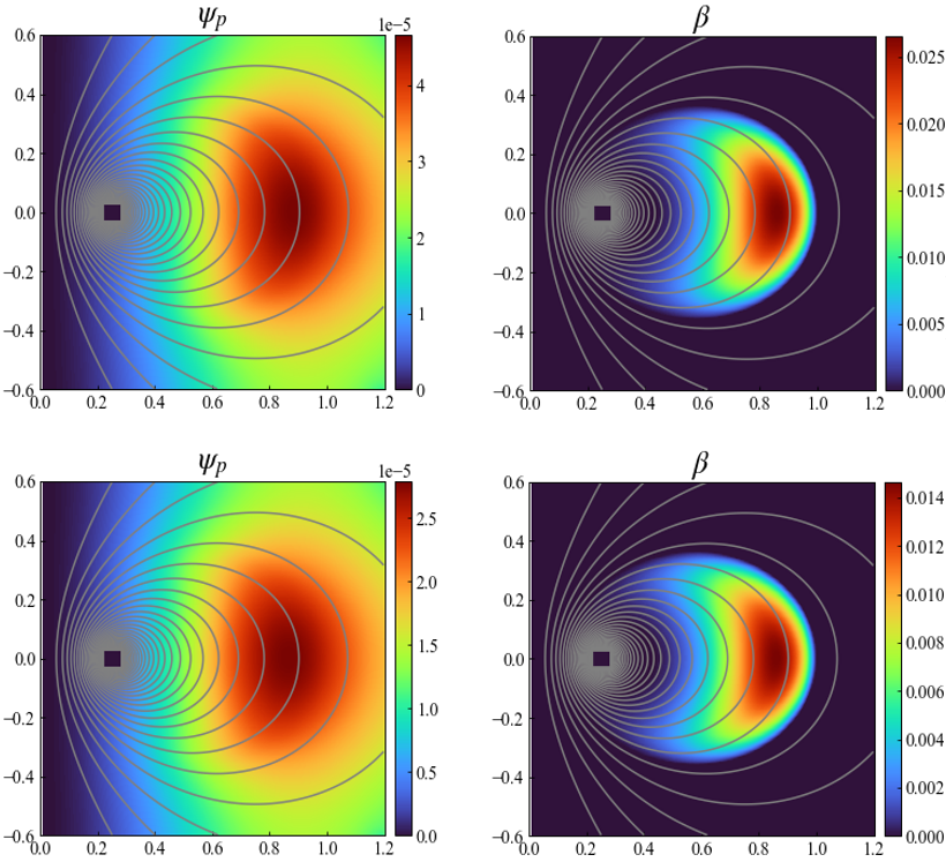

Figure 10.5: Distributions of ψ_p and β, which correspond to the equilibrium states calculated for $\beta_o = 4.5 \times 10^{-5}$ and (top) $\lambda_0 = 0.50$, (bottom) $\lambda_0 = 0.25$

Finally, we show the relations between λ_0 and β_o, and ψ_p. We can measure ψ_p using flux loops that orbit at constant r and z. Therefore, we can determine β_o and λ_0 using two flux loops (see fig. 10.6–10.8). Here, we set $r_1 = 1.01$, $z_1 = 0.35$, $z_2 = 0.20$.

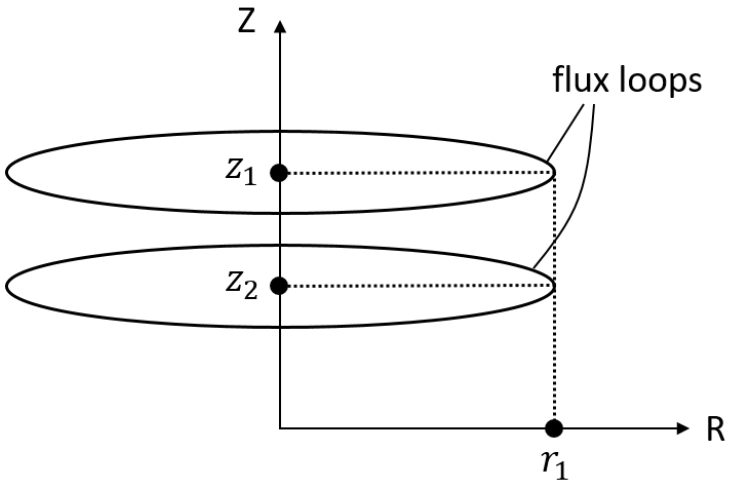

Figure 10.6: Schematic of the flux loops

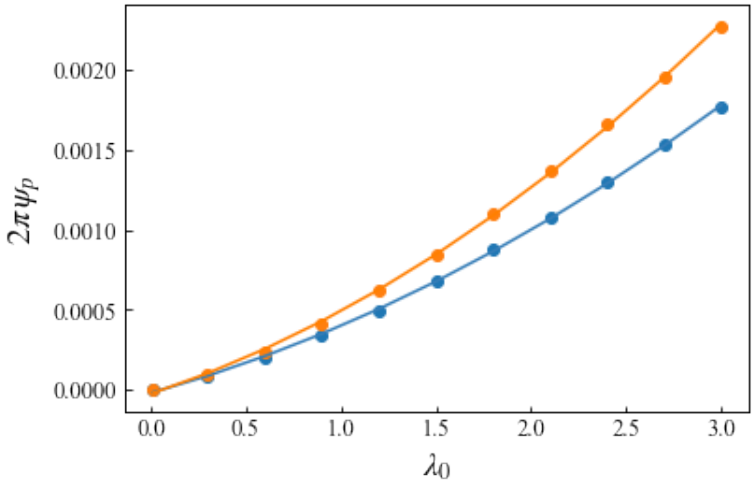

Figure 10.7: Relation between λ_0 and ψ_p where $\beta_o = 1.2 \times 10^{-5}$

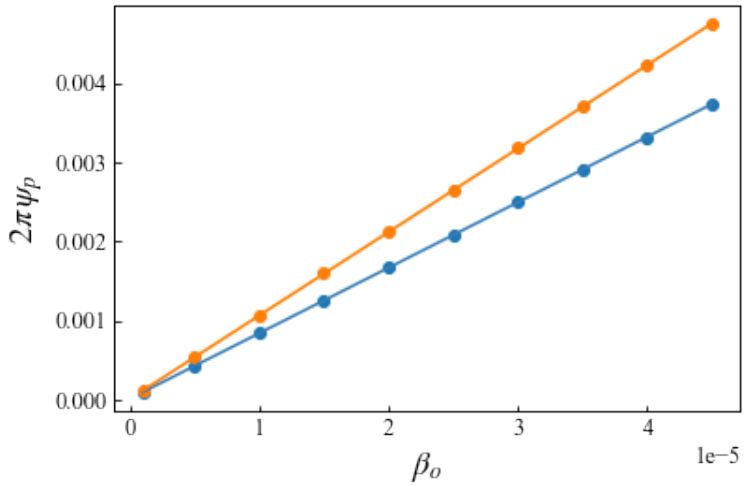

Figure 10.8: Relation between β_o and ψ_p where $\lambda_0 = 2.0$

Chapter 11

Conclusion of part II

To describe the high-beta equilibrium of a magnetospheric plasma, we need a consistent relation between the magnetic field (to be modified by the current in the plasma) and the phase-space distribution function (to be influenced by the magnetic field). The former is dictated by the field equation, and the latter is dictated by kinetic theory. We can use the (generalized) Grad–Shafranov equation as the field equation that determines the magnetic flux function for a given magnetization (diamagnetic) current. However, the Grad–Shafranov equation has an additional (in fact, essential) implication, that is, the internal relation between the magnetic field and the magnetization current, which is imposed by the magneto-fluid force–balance relation. Therefore, we need to find a special class of distribution functions that does not create inconsistencies with the macroscopic magneto-fluid model. In the present study, we showed that the "thermal equilibrium" on the topologically constrained phase space (foliated by the adiabatic invariant μ) is suitable for the generalized Grad–Shafranov equation, which is not only amenable, but also definitive for the functional form of the pressure tensor. However, we have left the flux function ψ as a free parameter that can control the "radial" profile of the pressure tensor. Hasegawa [40] suggested that $\partial_\psi f^* = 0$, because $P_\theta \sim \psi$ is the most fragile constant influenced by low-frequency ($\sim$ drift frequency) perturbation. In fact, we observe the "inward diffusion" of particles, consistent with the relaxation toward $\partial_\psi f^* = 0$ [42, 47]. However, in a real system, the boundaries (located both inside and outside the confinement domain) deform the distribution from the ideal one. In the present study, we maintained ψ as an

experimental parameter to model the nonequilibrium property.

Chapter 12

Conclusion of the paper

In this study, we focus on two self-organization phenomena in physical system: zonal flow and magnetospheric plasma. The central issue common to these two self-organization phenomena is how the self-organized states are determined. We consider that the constants of motion are the key to deal with the issue.

In part I, we estimate exact lower bounds on the 'zonal enstrophy' under the constraints of the constants of motion. By formulating the variational principle to estimate the lower bounds, we have found a discrete set of zonal enstrophy levels that are quantized by the eigen-value λ measuring the mode number, and verified that the estimated lower bounds give a reasonable estimate of the zonal enstrophy by comparing with simulation results. Here, the inequality of the constraints evoked by the non-coerciveness of the target functional is the interesting aspect of the variational principle. It is well-known that the inverse-cascade model explains the essence of the self-organization process of zonal flow in which the enstrophy cascades to small-scale vortices, while the energy tends to accumulate into large scales. Here, as a results of our study, we can reinterpret the process as a relaxation process where zonal enstrophy level is deexcited by the emission of short-scale wavy vorticity.

In part II we constructed the model to describe the high-beta equilibrium of a magnetospheric plasma which is consistent with the field equation ((generalized) Grad-Shafranov equation) and the kinetic theory. Here, constraints by the adiabatic invariant μ is essential to connect the kinetic theory to macro model described by generalized Grad-Shafranov

equation because scale hierarchy created by the constraint characterizes the macro-system. In this part, we showed that the “thermal equilibrium” on the topologically constrained phase space is suitable for the generalized Grad–Shafranov equation.

Appendix of part II

B Grand canonical ensemble

The function form of (8.7) implicitly assumes maximum entropy states under the appropriate constraints formulated in [52].

When we consider the grand canonical ensemble determined by the Casimir (magnetic moment) $C = \int \mu f^* \mathrm{d}^n z$ in addition to the total particle number $N = \int f^* \mathrm{d}^n z$ and total energy $E = \int H f^* \mathrm{d}^n z$, the equilibrium state in which entropy $S = -\int f^* \log f^* \mathrm{d}^n z$ is maximized is calculated as

$$\delta(S - \alpha N - \beta E - \gamma C) = 0, \tag{B.1}$$

which yields a Boltzmann distribution

$$f^* = Z^{-1} \exp(-\beta H - \gamma \mu), \tag{B.2}$$

where $Z := \exp(\alpha + 1)$ is the normalized factor and α, β, γ are Lagrange multipliers.

In our formulation, we also consider ψ as a constant of motion. Then, Z, β and γ can be the functions of ψ. However, in this study, we consider β to be a constant in (8.7) for simplicity.

When we do not consider the magnetic moment as a constraint, the equilibrium state obtained via entropy maximization changes drastically. The distribution function is obtained as

$$f^* = Z^{-1} \exp(-\beta H), \tag{B.3}$$

which is equivalent to the distribution function obtained by $T_{\parallel 0} = T_{\perp 0} = T_0$ in (8.7). The distribution function yields the pressure as

$$p_\parallel = p_\perp = A(\psi)\left(\frac{2\pi}{m}\right)^{\frac{3}{2}} T_{\parallel 0}^{\frac{5}{2}}, \tag{B.4}$$

which is isotropic and the function of ψ (not ψ and B). This simple exercise shows that the factor that causes the nontrivial structure along the magnetic field at the same time as entropy maximization is the constraint of the magnetic moment in the view of statistical mechanics.

C How to solve the Grad-Shafranov equation

Here, we review how we solved the Grad-Shafranov equation in part II. Our calculation was conducted based on a numerical code RTEQ (Ring Trap EQuilibrium) which had been developed mainly by Professor Furukawa[51].

C.1 Implementation of the solution using Green's function

We may rewrite eq.(9.4) as

$$\Delta^* \psi = -\mu_0 R J_t, \tag{C.5}$$

where $\mu_0 R J_t = \mu_0 R^2 \left.\dfrac{\partial p_\parallel}{\partial \psi}\right|_B + \dfrac{1}{\sigma}\nabla\psi \cdot \nabla\sigma$, and the boundary condition $\psi = 0$ at infinity is adopted. If J_t is independent of ψ, the solution of the equation is obtained analytically by using Green's function as

$$\psi = \int \mathrm{d}R'\mathrm{d}Z' G(R, Z|R', Z')\, \mu_0 J_t, \tag{C.6}$$

where

$$G(R, Z|R', Z') = \frac{1}{\pi}\sqrt{\frac{RR'}{k^2}}\left[\left(1 - \frac{k^2}{2}\right)K(k) - E(k)\right] \tag{C.7}$$

is Green's function and

$$k^2 := \frac{4RR'}{(R+R')^2 + (Z-Z')^2}, \tag{C.8}$$

$$K(k) := \int_0^{\pi/2} \frac{\mathrm{d}\theta}{\sqrt{1-k^2\sin^2\theta}} \tag{C.9}$$

$$E(k) := \int_0^{\pi/2} \mathrm{d}\theta \sqrt{1-k^2\sin^2\theta}. \tag{C.10}$$

Actually, however, J_t is a function of ψ. Thus, we have to calculate the solution numerically using iteration procedure.

C.2 Iteration procedure of RTEQ code

We show the flowchart of RTEQ code in fig.C.1. Firstly, we start from $\psi^{(0)}$ which corresponds to the vacuum magnetic field. Then, we iterate solving

$$\Delta^* \psi^{(n-)} = -\mu_0 R J_t(\psi^{(n-1)}) \tag{C.11}$$

and updating ψ as $\psi^{(n)} := \alpha\psi^{(n-)} + (1-\alpha)\psi^{(n-1)}$ until it converges. To solve (C.11), we just have to calculate (C.6) in principle. Actually, some methods to reduce calculation amount is applied in RTEQ code. In the evaluation of the convergence, we evaluate the inequality

$$\left| \frac{\psi^{(n-)} - \psi^{(n-1)}}{\psi^{(n-1)}} \right| < \epsilon. \tag{C.12}$$

In this study we set ϵ as $\epsilon = 10^{-8}$.

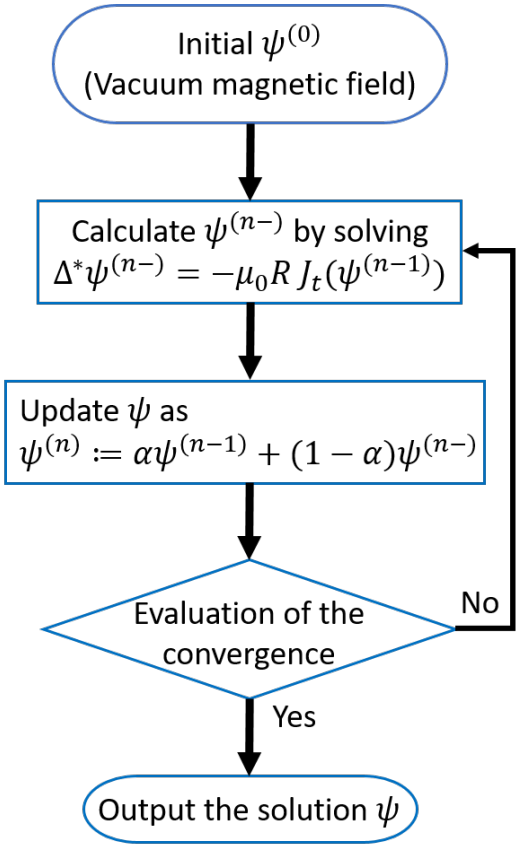

Figure C.1: The flowchart of RTEQ code.

Acknowledgements

First of all, I really appreciate for Professor Zensho Yoshida coaching me. He taught me not only plasma physics but also how to pursue the true nature of problems, how to build logic and how to describe the outcomes of our study in paper, presentation and so on. Moreover, his professionality as a scientist really motivated me. Although I think I brought him much trouble for lack of my ability and I still have a long way to go, his coaching for about three years really has made me grow.

I also appreciate Saitoh associate professor, Nishiura associate professor, Kenmochi assistant professor, Sato assistant professor, Kitayama-san and all members of the laboratory. I am grateful to Saitoh associate professor for undertaking my supervisor as a substitute for Prof. Yoshida since April, 2021. Discussion with the members of the laboratory really help me deepen my thoughts and was very enjoyable. Especially, discussion with K. Ueda was very important for the contents of part II. Support by Kitayama-san was very helpful for me to concentrate on the study in my graduate school life. I also appreciate Yamazaki-san and Hashimoto-san of Department of Advanced Energy supporting my graduate school life, too.

I appreciate Kawazura assistant professor and Furukawa associate professor, too. The study of part I and part II is established thanks to the code programed by them, respectively.

Lastly, I greatly appreciate for my parents supporting me to study in the graduate school.

Hiroto Aibara

Bibliography

[1] F. Wagner, G. Becker, and et al. K. Behringer. Regime of improved confinement and high beta in neutral-beam-heated divertor discharges of the asdex tokamak. *Physical Review Letters*, 49(19):1408, 1982.

[2] 小林すみれ. 臨界状態プラズマ乱流における帯状流と乱流の相互作用. **プラズマ・核融合学会誌**, 92(3):211–217, 2016.

[3] H. Aibara and Z. Yoshida. Lower bounds on zonal enstrophy. *Journal of Fluid Mechanics*, 919, 2021.

[4] H. Aibara, Z. Yoshida, and K. Shirahata. Kinetic construction of the high-beta anisotropic-pressure equilibrium. *arXiv preprint arXiv:2108.12968*, 2021.

[5] J. G. Charney. Geostrophic turbulence. *J. Atmos. Sci.*, 28:1087–1095, 1971.

[6] A. Hasegawa. Self-organization processes in continuous media. *Ad. Phys.*, 34:1–42, 1985.

[7] P. H. Diamond, S.-I. Itoh, K. Itoh, and T.S. Hahm. Zonal flows in plasma —a review. *Plasma Phys. Control. Fusion.*, 47:R35–R161, 2005.

[8] R. H. Kraichnan. Inertial ranges in two-dimensional turbulence. *Phys. Fluids*, 10:1417–1423, 1967.

[9] P. B. Rhines. Waves and turbulence on a beta-plane. *J. Fluid Mech.*, 69:417–443, 1975.

[10] E. N. Lorentz. Barotropic instability of rossby wave motion. *J. Atmos. Sci.*, 29:258–265, 1972.

[11] A. E. Gill. The stability of planetary waves on an infinite beta-plane. *Geophys. Fluid Dyn.*, 6:29–47, 1974.

[12] C. Connaughton, B. Nadiga, S. Nazarenko, and B. Quinn. Modulational instability of rossby and drift waves and generation of zonal jets. *J. Fluid Mech.*, 654:207–231, 2010.

[13] A. M. Balk, S. V. Nazarenko, and V. E. Zakharov. New invariant for drift turbulence. *Phys. Lett. A*, 152:276–280, 1991.

[14] A. M. Balk. New invariant for rossby wave systems. *Phys. Lett. A*, 155:20–24, 1991.

[15] A. M. Balk. Angular distribution of rossby wave energy. *Phys. Lett. A*, 345:154–160, 2005.

[16] B. F. Farrell and P. J. Ioannou. Structure and spacing of jets in barotropic turbulence. *J. Atmos. Sci.*, 64:3652–3665, 2007.

[17] N. A. Bakas and P. J. Ioannou. Structural stability theory of two-dimensional fluid flow under stochastic forcing. *J. Fluid Mech.*, 682:332–361, 2011.

[18] K. Srinivasan and W. R. Young. Zonostrophic instability. *J. Atmos. Sci.*, 69:1633–1656, 2012.

[19] D. G. Dritschel and M. E. McIntyre. Multiple jets as pv staircases: the phillips effect and the resilience of eddy-transport barriers. *J. Atmos. Sci.*, 65:855–874, 2008.

[20] R. K. Scott and D. G. Dritschel. The structure of zonal jets in geostrophic turbulence. *J. Fluid Mech.*, 711:576–598, 2012.

[21] S. Yoden and M. Yamada. A numerical experiment on two-dimensional decaying turbulence on a rotating sphere. *J. Atmos. Sci.*, 50:631–644, 1993.

[22] G. K. Vallis and M. E. Maltrud. Generation of mean flows and jets on a beta plane and over topography. *J. Phys. Oceanogr.*, 23:1346–1362, 1993.

[23] S. Yoden, K. Ihioka, Y.-Y. Hayashi, and M. Yamada. A further experiment on two-dimensional decaying turbulence on a rotating sphere. *Il nuovo cimento C*, 22:803–812, 1999.

[24] G. P. Williams. Planetary circulations: 1. barotropic representation of jovian and terrestrial turbulence. *J. Atmos. Sci.*, 35:1399–1426, 1978.

[25] S. Danilov and D. Gurarie. Rhines scale and spectra of the beta-plane turbulence with bottom drag. *PHYSICAL REVIEW E*, 65:067301, 2002.

[26] S. Sukoriansky, N. Dikovskaya, and B. Galperin. On the arrest of inverse energy cascade and the rhines scale. *J. Atmos. Sci.*, 64:3312–3327, 2007.

[27] N. Ito and Z. Yoshida. Statistical mechanics of magnetohydrodynamics. *Phys. Rev. E*, 53:5200–5206, 1996.

[28] J. Miller. Statistical mechanics of euler equations in two dimensions. *Physical review letters*, 65(17):2137–2140, 1990.

[29] R. Robert and J. Sommeria. Statistical equilibrium states for two-dimensional flows. *Journal of Fluid Mechanics*, 229:291–310, 1991.

[30] B. Turkington, A. Majda, K. Haven, and M. Dibattista. Statistical equilibrium predictions of jets and spots on jupiter. *PNAS*, 98:12346–12350, 2001.

[31] J. B. Taylor. Relaxation of toroidal plasma and generation of reverse magnetic fields. *Phys. Rev. Lett.*, 33:1139–1141, 1974.

[32] J. B. Taylor. Relaxation and magnetic reconnection in plasmas. *Rev. Mod. Phys.*, 58:741–763, 1986.

[33] F. P. Bretherton and D. B. Haidvogel. Two-dimensional turbulence above topography. *J. Fluid Mech.*, 78(1):129–154, 1976.

[34] P. J. Morrison. Hamiltonian description of the ideal fluid. *Rev. Mod. Phys.*, 70:467–521, 1998.

[35] T. Shepherd. Rigorous bounds on the nonlinear saturation of instabilities to parallel shear flows. *J. Fluid Mech.*, 196:291–322, 1988.

[36] K. Ishioka and S. Yoden. Numerical methods of estimating bounds on the non-linear saturation of barotropic instability. *J. Met. Soc. Jpn. Ser. II*, 74:167–174, 1996.

[37] Jacques Louis Lions and Enrico Magenes. *Non-homogeneous boundary value problems and applications*, volume 1. Springer Science & Business Media, 2012.

[38] Z. Yoshida and S. M. Mahajan. Variational principles and self-organization in two-fluid plasmas. *Phys. Rev. Lett.*, 88:095001, 2002.

[39] S. M. Krimigis, T.P Armstrong, and et al. W. I. Axford. Hot plasma environment at jupiter: Voyager 2 results. *Science*, 206(4421):977–984, 1979.

[40] A. Hasegawa. A dipole field fusion reactor, 1987.

[41] A. Hasegawa, L. Chen, and M. E. Mauel. A d-3he fusion reactor based on a dipole magnetic field. *Nuclear Fusion*, 30(11):2405, 1990.

[42] D. T. Garnier, A. C. Boxer, and et al. J. L. Ellsworth. Confinement improvement with magnetic levitation of a superconducting dipole. *Nuclear fusion*, 49(5):055023, 2009.

[43] Z. Yoshida, Y. Ogawa, and et al. J. Morikawa. First plasma in the rt-1 device. *Plasma and Fusion Research*, 1:008–008, 2006.

[44] H. Saitoh, Z. Yoshida, and et al. J. Morikawa. Formation of high-β plasma and stable confinement of toroidal electron plasma in ring trap 1. *Physics of plasmas*, 18(5):056102, 2011.

[45] Z. Yoshida, Y. Yano, J. Morikawa, and H. Saitoh. Thermo-magneto coupling in a dipole plasma. *Physics of Plasmas*, 19(7):072303, 2012.

[46] H. Grad and H. Rubin. Proceedings of the second united nations international conference on the peaceful uses of atomic energy. 1958.

[47] Y. Kawazura, Z. Yoshida, and et al. M. Nishiura. Observation of particle acceleration in laboratory magnetosphere. *Physics of Plasmas*, 22(11):112503, 2015.

[48] Harold Grad. *Proceedings of Symposia in Applied Mathematics*. 1967.

[49] H. Grad. Toroidal containment of a plasma. *The Physics of Fluids*, 10(1):137–154, 1967.

[50] S. I. Krasheninnikov and P. J. Catto. Effects of pressure anisotropy on plasma equilibrium in the magnetic field of a point dipole. *Physics of Plasmas*, 7(2):626–628, 2000.

[51] M. Furukawa. Effects of pressure anisotropy on magnetospheric magnetohydrodynamics equilibrium of an internal ring current system. *Physics of Plasmas*, 21(1):012511, 2014.

[52] Z. Yoshida and S. M. Mahajan. Self-organization in foliated phase space: Construction of a scale hierarchy by adiabatic invariants of magnetized particles. *Progress of Theoretical and Experimental Physics*, 2014(7):073J01, 2014.

Publication

Article

Lower bounds on zonal enstrophy.,
H. Aibara and Z. Yoshida, Journal of Fluid Mechanics 919 (2021).

Kinetic construction of the high-beta anisotropic-pressure equilibrium.,
H. Aibara, Z. Yoshida and K. Shirahata, arXiv preprint arXiv:2108.12968 (2021).

Presentation

The partition of enstrophy between zonal and turbulent components,
H. Aibara and Z. Yoshida, 3rd Asia Pacific Conference on Plasma Physics, F-O1, Hefei, China (November, 2019)

離散化されたエンストロフィーレベルと緩和過程：変分原理から見た帯状流の自己組織化,
相原 寛人, 吉田 善章, 日本物理学会 2020 年秋季大会, 9pB1-3, zoom meeting (2020 年 9 月)

帯状流に分配されるエンストロフィーの変分原理による評価,
相原 寛人, 吉田 善章, 日本流体力学会 年会 2020, 045, zoom meeting (2020 年 9 月)

Discrete enstrophy levels and the relaxation process: Self-organizationof zonal flow in the view of variational principle,
H. Aibara and Z. Yoshida, 4th Asia Pacific Conference on Plasma Physics (Invited), F-I8, zoom meeting (October, 2020)

(発表予定) 運動論に基づいた磁気圏プラズマ高ベータ平衡の構築,
相原 寛人, 吉田 善章, 上田研二, 日本物理学会 2021 年秋季大会, 20aB1-12, zoom meeting (2021 年 9 月)